AD-A095 414 DREXEL UNIV PHILADELPHIA PA COLL OF ENGINEERING F/G 11/6
MELT PURIFICATION VIA FILTRATION.(U)
OCT 80 D APELIAN, R MUTHARASAN, C ROMANOWSKI DAAG46-79-C-0052
UNCLASSIFIED AMMRC-TR-80-49 NL

1 OF 1
AD
A095 414

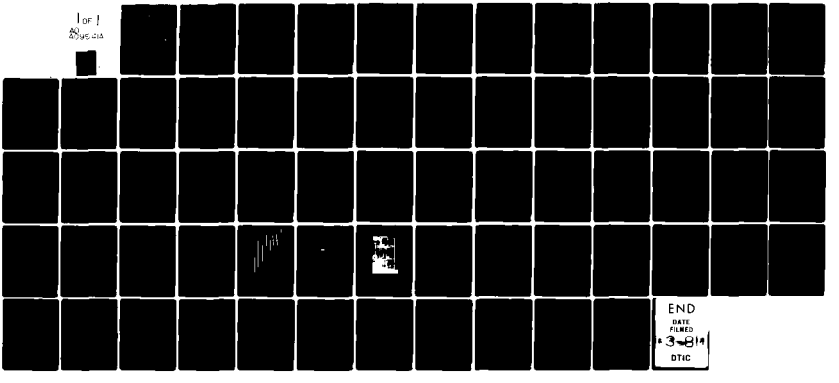

END
DATE FILMED
3-81
DTIC

12

43

AD

LEVEL III

AD A095414

AMMRC TR 80-49

MELT PURIFICATION VIA FILTRATION

OCTOBER 1980

D. APELIAN, R. MUTHARASAN AND C. ROMANOWSKI

COLLEGE OF ENGINEERING
DREXEL UNIVERSITY
PHILADELPHIA, PA 19104

Interim Report Contract Number: DAAG46-79-C-0052

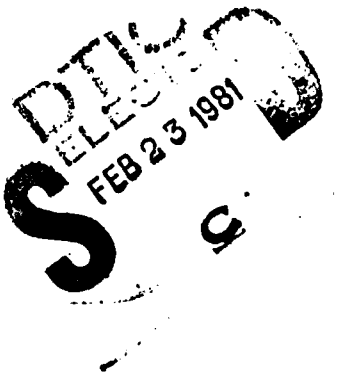

Approved for public release; distribution unlimited.

Prepared for

ARMY MATERIALS AND MECHANICS RESEARCH CENTER
Watertown, Massachusetts 02172

The findings in this report are not to be construed as an official Department of the Army position, unless so designated by other authorized documents.

Mention of any trade names or manufacturers in this report shall not be construed as advertising nor as an official indorsement or approval of such products or companies by the United States Government.

DISPOSITION INSTRUCTIONS

Destroy this report when it is no longer needed.
Do not return it to the originator.

SECURITY CLASSIFICATION OF THIS PAGE (When Data Entered)

REPORT DOCUMENTATION PAGE

READ INSTRUCTIONS BEFORE COMPLETING FORM

1. REPORT NUMBER: AMMRC TR-80-49	2. GOVT ACCESSION NO.: AD-A095 414
3. RECIPIENT'S CATALOG NUMBER:	
4. TITLE (and Subtitle): Melt Purification via Filtration,	5. TYPE OF REPORT & PERIOD COVERED: Interim Report 1/1/80-7/1/80
	6. PERFORMING ORG. REPORT NUMBER:
7. AUTHOR(s): D. Apelian, R. Mutharasan and C. Romanowski	8. CONTRACT OR GRANT NUMBER(s): DAAG46-79-C-0052
9. PERFORMING ORGANIZATION NAME AND ADDRESS: College of Engineering, Drexel University, Philadelphia, PA 19104	10. PROGRAM ELEMENT, PROJECT, TASK AREA & WORK UNIT NUMBERS: D/A Project: 1L162105AH84; AMCMS Code: 612105 H 84001; Agency Accession: DA064778
11. CONTROLLING OFFICE NAME AND ADDRESS: Army Materials and Mechanics Research Center, Watertown, Massachusetts 02172	12. REPORT DATE: October 1980
	13. NUMBER OF PAGES: 62
14. MONITORING AGENCY NAME & ADDRESS (if different from Controlling Office)	15. SECURITY CLASS. (of this report): Unclassified
	15a. DECLASSIFICATION/DOWNGRADING SCHEDULE

16. DISTRIBUTION STATEMENT (of this Report)

Approved for public release; distribution unlimited.

17. DISTRIBUTION STATEMENT (of the abstract entered in Block 20, if different from Report)

18. SUPPLEMENTARY NOTES

19. KEY WORDS (Continue on reverse side if necessary and identify by block number)

Filtration
Liquid Metals
Aluminum
Steel
Superalloys
Purification

20. ABSTRACT

Background on the mechanisms and kinetics of filtration is discussed and the mathematical model of liquid metal filtration proposed by Drexel is updated and further elaborated.

The study using the apparatus developed for molten aluminum filtration has been extended to characterize the effect of filter media. The steel filtration apparatus and initial experimentation are described. The Low Temperature Model study has been completed and is described and discussed.

Reference is made to future work in Aluminum and Steel filtration, another low temperature model and a math-model Inclusion Flow Trajectory.

DD FORM 1 JAN 73 1473 EDITION OF 1 NOV 65 IS OBSOLETE

Unclassified

SECURITY CLASSIFICATION OF THIS PAGE (When Data Entered)

ABSTRACT

Background on the mechanisms and kinetics of filtration is discussed and the mathematical model of liquid metal filtration proposed by Drexel is updated and further elaborated.

The study using the apparatus developed for molten aluminum filtration has been extended to characterize the effect of filter media. The steel filtration apparatus and initial experimentation are described. The Low Temperature Model study has been completed and is described and discussed.

Reference is made to future work in Aluminum and Steel filtration, as well as another low temperature model and a study to mathematically predict Inclusion Flow Trajectory.

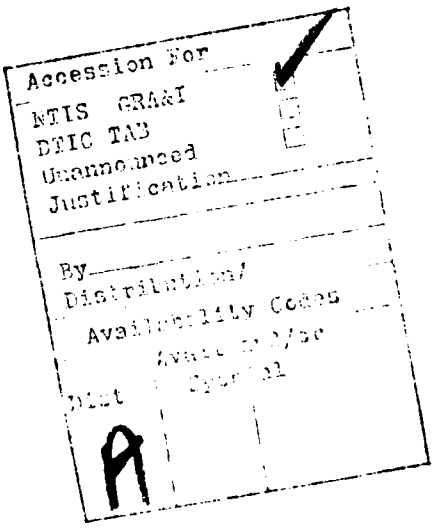

FOREWORD

This report was prepared by Drexel University summarizing the progress during the second six months on the feasibility of inclusion removal from molten metal systems. The contract, DAAG46-79-C0052 is being administered under the direction of Mr. Arthur Ayvazian of the U. S. Army Materials and Mechanics Research Center, Watertown, Massachusetts.

TABLE OF CONTENTS

1. INTRODUCTION

The objective of this work is to characterize, improve and develop molten metal filtering techniques, with particular reference to the feasibility of purifying aluminum, steel and nickel based superalloys and to evaluate the resulting property improvements.

The reason for filtering liquid metals is to remove impurities present in the melt either as solid or liquid particles. It is financially and economically advantageous to remove these particles as they are known to reduce fluidity of the melt, cause internal porosity in castings, reduce mechanical strength, ductility and fatigue resistance of the product and also result in poor machinability, surface, finish, etc.

The particles present in molten metal prior to casting are an inevitable feature of the production route and may be characterized as:

i) Exogenous inclusions: these are either unavoidably present, such as refractory particles, or may be inadvertently added such as coarse clusters of grain refiner, etc.

ii) Deoxidation products and salts: these are suspended in the melt as the result of a prior metal treatment process e.g. Al_2O_3 or SiO_2 deoxidation products in steel, or light metal halide salts after reacting gas "cleaning" of aluminum.

iii) Oxide of the melt which is both suspended on top of the melt and is entrapped within it due to turbulance e.g. Al_2O_3 in aluminum melts.

It has been found from industrial observation that the majority of the above particles which are deleterious to product quality lie in the range of 1 - 30μm diameter and are dilutely suspended (about 0.03% in steel).

The most efficient and commercially attractive way of removing the above inclusions is by filtration prior to casting - passing the liquid metal through a packed bed of refractory particles [1], screens[2], ceramic foam filters[3] and other media. Filtration of aluminum and its alloys has been a commercial reality for many years; work being pioneered by Brondyke and Hess of Alcoa[4] and Brant, Bone and Emley of British Aluminium.

2. BACKGROUND

Due to the experimental difficulties involved (high temperatures) and the inherent constraints of the filtration process, previous investigations of liquid metal filtration have been limited to indirect evaluation through the differences in specific properties of filtered and unfiltered metals. Consequently, process design to-date has largely consisted of a plant oriented trial and error approach.

The ultimate aim of this program therefore, is not only to establish the feasibility, but also to quantitatively compare filter media, and to identify and characterize the process variables and capture mechanisms which affect filtration efficiency and kinetics.

There are two well-known mechanisms of filtration (i) surface filtration and (ii) deep bed filtration. Surface filtration is normally used for high-solid suspensions, while deep bed filters are used for dilute ones (0.01 to 0.05 vol. %). Surface filtration relies on cake formation for particle retention and hence, the size of the filter pores must be smaller than that of the impurities. This requires high operating pressures and thus surface filtration is impractical for most metallurgical applications. On the other hand, a depth filter disperses the inclusions through part or all of its volume (depth). It thus has the advantage of having a large surface area for entrapment and can trap particles much smaller than the pores of the filter bed. Depth filters are therefore, more suitable for metallurgical applications. Consequently, it was decided that the initial part of this investigation should

concentrate on depth filtration.

In order that a rigorous, systematic study of liquid metal filtration (both ferrous and non-ferrous) could be performed, the necessary experimental apparatus and expertise had to be developed. From the experimental viewpoint the filtration of aluminum was the least difficult of the three proposed alloy systems, hence it was the first task to be addressed. A large number of depth filtration trials were made using the aluminum-titanium diboride system. Using the experience gained from this work a steel filtration apparatus was designed.

A theoretical model was proposed and compared with the results from the first phase of this investigation. Good correlation was noted and conclusions were drawn as to the inclusion removal rate and efficiency as a function of melt flow rate. To further characterize these parameters a low temperature model study was investigated. All this initial work has been fully detailed in the preceeding report (AMMRC TR-80-160).

Since this initial work, the aluminum/titanium diboride study has been extended to encompass variations in filter characteristics such as porosity, length of bed, filter area, etc. By understanding the effect of these fundamental parameters on inclusion capture behavior and capture kinetics, it is possible to begin establishing the criteria for optimization. Also, since the last report the low temperature model work has been pursued with interesting results and the steel filtration apparatus has been completed and commissioned. Further details of progress in all three fields of activity may be found in section 5. The combined results obtained from this work have allowed the proposed kinetic model to be further refined and updated and this is described in the following section.

3. PROPOSED KINETIC MODEL

The model described in the preceeding report has been slightly revised so that it may more effectively describe and quantify the important variables and parameters affecting the inclusion removal kinetics and filtration efficiency. This model, as described below, agrees closely with the experimental results obtained in the extension of the aluminum-titanium diboride work (see section 5.1). Thus, in conjunction with experimental work the model enables the prediction of filtration processes, hence allowing the optimization of filter design for any specific melt system. The model is, at present, limited to the short-term behavior of the filter, a situation which reflects the experimental runs. The fundamental mechanisms, however, remain largely the same throughout the majority of a filter's useful life and are described below.

When a melt containing inclusions flows past the grains of the filter medium, the inclusions deposit on the surface of the grain due to diffusion direct interception, gravity, and/or surface forces. Mechanical entrapment has been observed to be responsible for filtration of inclusions larger than 30μm; whereas, it is believed that surface forces are responsible for the retention of inclusions smaller than 30μm. The primary mode of transport of inclusions smaller than 30μm to the grain surface of the filter medium is due to flow dynamics, while surface forces are responsible for retention of the inclusion.

When a filter is exposed to a melt containing inclusions, the inclusions become entrapped on the surface of the filter grains. The rate of change of entrapped inclusions per unit packing volume, $\frac{\partial \sigma}{\partial \tau}$, is a function of inclusion concentration in the melt[6]. That is,

$$\frac{\partial \sigma}{\partial \tau} = KC \qquad (1)$$

where K is the kinetic parameter, C is the inclusion concentration in the melt and τ is the characteristic time. In general K may be a function of σ, which is the concentration of entrapped inclusions, as well as a function of the melt physical properties, melt flow rate and the shape and size of the inclusions. The functional nature of K may be expressed as[6]

$$K = K_o \left(1 - \frac{\sigma}{\sigma_m}\right) \tag{2}$$

where K_o is the kinetic parameter coefficient and σ_m is the inclusion retention capacity of the filter bed. Use of the above kinetic expression, Eq. (2), in conjunction with an inclusion mass balance over a differential filter (see Figure 1) results in a first order partial differential equation[6]. Using the appropriate boundary conditions the solution can be obtained as

$$\frac{C}{C_i} = \frac{\exp\left[\frac{C_i}{\sigma_m}\ \varepsilon_i\ \phi\ (\theta - \eta)\right]}{\exp(\phi\eta) + \exp\left[\frac{C_i}{\sigma_m}\ \varepsilon_i\ \phi\ (\theta - \eta)\right] - 1} \tag{3}$$

where the subscript i refers to the inlet condition and the dimensionless parameters are:

$$\theta = \frac{t\ U_m}{\varepsilon_i L}\ , \text{ dimensionless time} \tag{4}$$

$$\eta = \frac{Z}{L}\ , \text{ dimensionless distance} \tag{5}$$

$$\phi = \frac{K_o L}{U_m}\ , \text{ dimensionless kinetic constant} \tag{6}$$

In the above expression, ε_i is the bed porosity, t is time, U_m is the melt approach velocity, L is the height of filter bed and Z is the distance from the filter entrance.

Equation (3) gives the concentration of inclusions in the melt as a function of time and distance along the filter. For a given value of θ, Eq. (3) describes the axial composition profile. If one is interested in the exit concentration, then η will be set to unity in Eq. (3) and the resulting expression gives the outlet inclusion concentration, C_o as a function of time.

The fundamental parameter which characterizes the performance of a depth filter is the kinetic parameter K, as given by Eq. (2). However, the value of K is a function of the magnitude of the coefficient K_o and the relative bed retention, σ/σ_m (see Eq. (2)). The coefficient K_o is a function of the melt velocity through the filter, U_m, the inclusion size, d_i, the filter grain size, d_g, and the melt system. The coefficient K_o can be experimentally determined by short time experiments, whereas determination of σ_m would require experiments of long duration.

A filter having a relatively finite capacity for inclusions, will reach maximum inclusion retention capacity with extended use. On the other hand, for a filter having a very large capacity for inclusions, progressive blockage of melt flow will occur with extended use. To determine the inclusion retention capacity factor, σ_m, melts in the order of thousands of pounds must be filtered and hence would require pilot-plant scale equipment. In this study the coefficient K_o has been experimentally determined and its dependence on melt velocity has been quantified using a model melt system ($Al\text{-}TiB_2$).

During the initial stages of filter use when the filter bed has been exposed to only a few residence times, the inclusion retention capacity value of the filter is large compared to the entrapped inclusions, that is,

$\sigma/\sigma_M \rightarrow 0$. Under this condition, it can be shown that

$$\frac{C_i}{\sigma_m} \varepsilon_i \phi \ (\theta - \eta) \rightarrow 0. \tag{7}$$

The above enables us to simplify equation (3) to

$$\frac{C(Z)}{C_i} = \exp (- \phi\eta) = \exp (- \frac{K_o Z}{U_m}) \tag{8}$$

At the exit end of the filter, the dimensionless distance, $\eta = 1$ and the above expression reduces to

$$\frac{C_o}{C_i} = \exp \ (- \frac{K_o L}{U_m}) \tag{9}$$

Experiments can be designed to measure C_i, C_o, U_m and L, and thus K_o can be calculated by the use of Equation (9). The preferred approach is one in which data from many experiments can be used collectively to determine the coefficient K_o. Rearrangement of Equation (9) gives

$$\frac{1}{U_m} = \frac{1}{K_o L} \ln (\frac{C_i}{C_o}) \tag{10}$$

The above suggests that if K_o is not a function of the melt velocity, U_m, then a plot of $1/U_m$ vs. $\ln (C_i/C_o)$ will yield a straight line with a slope of $1/K_o L$ passing through the origin. From the slope of the graph one can calculate the coefficient K_o. However, if the assumption that K_o is independent of the melt velocity cannot be made, one may express the dependence of K_o on U_m to the first order approximation as a linear function

such as

$$K_o = K_o' + K_o'' U_m \tag{11}$$

Combining the above with Eq. (9)

$$\frac{1}{U_m} = \frac{1}{K'_o L} \ln \left(\frac{C_o}{C_i} \right) + \left(- \frac{K_o''}{K_o'} \right) \tag{12}$$

The above suggests that a plot of $1/U_m$ vs $\ln (C_i/C_o)$ will also give a straight line with an intercept of value $(- K_o''/K_o')$ and a slope of $1/K_o'L$. Hence, the two parameters K_o' and K_o'' can be calculated from the plot of $1/U_m$ vs $\ln (C_i/C_o)$.

It can be seen from Eq. (11) that the capture kinetics are a function of two terms: the first a constant, attributable to the characteristics of the filter bed i.e. filter media size and type, bed porosity and tortuosity, flow geometry, etc; whilst the second is a variable which modulates the expression for flow rate.

The model may be rearranged to accommodate an experimental technique where filtered samples are taken along the length of the filter bed; that is, inclusion concentration C, as a function of height, Z is measured. Equation (9) can be rearranged as

$$\ln \left(\frac{C_i}{C(Z)} \right) = \frac{U_m}{K_o} \quad Z \tag{13}$$

A plot of $\ln(C_i/C(Z))$ as a function of Z will yield a straight line with a slope of U_m/K_o and passing through the origin. In this approach one need not make the assumption on the functional dependence of K_o on the melt velocity U_m. Here, a single short-time filtration experiment will enable the determination of the kinetic parameter K_o.

Of the two experimental approaches described, it is experimentally easier to use the first method for melt systems in which only the outlet and inlet samples are monitored. However, the second approach is found to be effective in the low temperature model system studies.

4. RESEARCH OBJECTIVES

The goal of the proposed program is to study and evaluate the feasibility and utility of purifying liquid metal by filtering it prior to casting. More specifically, the various tasks that need to be investigated are:

- evaluate various filter media in terms of serviceability and compatibility.
- model the filtration process for liquid metals to quantify the particle capture kinetics.
- develop the required process parameters, i.e., approach velocity of the melt, porosity of the filter bed and pressure drop characteristics.
- optimum design of the filter for specific alloy systems such as aluminum, deoxidized steel, and superalloys.
- evaluate the mechanical properties of the filtered metal-reduction of area, tensile, impact and fatigue properties.

The program schedule is shown in Figure 2.

5. PROGRESS TO DATE

The filtration work with the aluminum-titanium diboride system has continued and been extended to include various bed heights, areas and

filter media. The steel filtration apparatus, whose design was based on the experience gained with aluminum filtration, has been completed and initial scoping runs have been performed. The concept of using a low temperature model system, discussed in the previous report, has come to practical fruition: the results giving a more complete characterization of the mechanisms involved in the filtration of molten metals. Although the low temperature study has been taken to a logical end point, work in the other two investigations is still ongoing. Each of the three activities is further discussed below.

5.1 Aluminum Filtration

The experimental apparatus takes into account the corrosive nature of molten aluminum, the requirements of sustained heating, adequate filter depth and metal flow rates in the range of 1-17 kg/m^2.s) i.e. filter factors of 5-90 lbs./in^{2}hr. The apparatus consists of the filter bed contained within a tube (either refractory or refractory coated steel) placed in a resistance furnace with an orifice at the bottom to control the flow rate. The well stirred melt containing synthetic tracer inclusions of TiB_2 (chosen for their size range, availability and ease of analysis) is poured into the pre-infiltrated filter bed in such a way that a constant metallostatic head is maintained. Inlet and filtered outlet samples are obtained for flow rate and TiB_2 analysis. It is assumed that at the filtration temperature all of the boron present is chemically bound to the titanium. (A more detailed account of the experimental apparatus and method may be found in AMMRC TR-80-16).

In the initial work all the filtration runs were performed using 3 to 4 mm. tabular alumina (standard industrial grade) as the filter medium. The current phase of the study has now been extended to include variations in filter medium, size, length, area and it is expected that future work will evaluate several other candidate media with suitable inertness, thermal shock resistance, erosion behavior, wetting properties, etc.

The current phase of the work has investigated six different types of filter bed arrangement:

i) 2 inch layer of 1/2 inch dia. alumina balls

ii) 10 inch layer of 1/2 inch dia. alumina balls

iii) 10 inch layer of 1-3 mm. tabular alumina

iv) 2 inch layer of 1-3 mm. tabular alumina

v) a bed as in (iv) but of reduced cross sectional area (1.5 sq. ins. as opposed to 12.6 sq.ins.)

vi) a sandwich arrangement of (i) + (iii) + (i) for comparison with the earlier work.

Although the results of this work are still to be fully analyzed, preliminary results and discussion are presented in section 6.1.

5.2 Steel Filtration Apparatus

Using the experience gained in the aluminum filtration, a steel filtration apparatus was designed and constructed. A schematic plan of the apparatus is shown in Figure 3 and a photograph of the finished equipment is shown in Figure 4. The apparatus consists of an outer pressure vessel which is divided into two compartments. The upper half houses the alumina crucible which contains the filter bed and the melt (charge) to be filtered. The crucible is heated by induction via susceptors. The filter bed consists of tabular alumina particles of 3 to 4 mm in diameter. The bed itself is 50 mm in diameter and its height can be varied up to 350 mm. To prevent the alumina particles from floating they are restrained by an alumina disk with orifices for the melt to flow through. At the underside, the filter bed is supported by another alumina disk with a predetermined size orifice which restricts and controls melt flowrate through the bed. The lower half of the vessel contains the mold which will subsequently receive the filtered melt. The weight of the crucible is monitored by a load cell so that one can accurately determine

the instantaneous flowrate of the filtered melt. Both chambers of the apparatus may be evacuated or exposed to argon at similar or differing pressures, the values of which are recorded by pressure indicators connected to each chamber.

The experimental procedure is as follows: The melt is prepared by charging 4Kg of electrolytic iron with a known oxygen level into the crucible. The chambers are evacuated and a constant argon purge is introduced. The charge is then heated by induction until a melt temperature of 1870°K is attained. A predetermined amount of aluminum is then charged into the crucible. This is accomplished by holding the aluminum under the liquid iron surface with a length of refractory; the aluminum quickly melts and dissolves under the rigorous stirring effect of the electromagnetic field.

The literature indicates that Al_2O_3 is the primary deoxidation product when the oxygen level of the melt is less than 0.058%, while at higher oxygen levels hercynite forms[7]. Initial work with this apparatus consisted of the deoxidation products being categorized. It was found that difficulties arose with metallographically identifying the primary (i.e. present in solution prior to the onset of solidification) deoxidation products, from any secondary inclusions that may form after the melt has been filtered. Consequently, work is currently in progress to investigate the possibility of adding small quantities of a substitutional alloying element e.g. Nickel or Phosphorus, in order to define more clearly the as cast microstructure. Also, a sampling technique for the experimental setup is under development: various samples are under evaluation and also the possibility of leaving a known quantity of the metal above the filter for bulk analysis is being considered. Once these initial inclusion characterization experiments are completed a melt with known inclusions can be prepared. This can be caused to flow through the filter by an argon pressure differential of 20 to 40 p.s.i. applied between the two chambers. When all the melt flows through the filter the pressure between the two chambers is equalized indicating the end of the run.

Filtration performance is evaluated by analyzing inlet and outlet samples for soluble and insoluble aluminum and total oxygen content. Thanks to Dr. Harry Paxton of U. S. Steel Laboratories, the chemical analyses are being evaluated at U. S. Steel's laboratories. Methods of analyzing size distribution of filtered and unfiltered melt inclusions are being looked into to establish the size range of inclusions being removed as this factor is not reflected in the normal quantitative analysis.

Some scoping filtration runs have already been made and the results from these are presented and discussed in section 6.2.

5.3 The Low Temperature Model System

This was an added task; however it was felt that the data obtained through this model system would be extremely valuable in obtaining a more complete characterization of the mechanisms involved in the filtration of molten metals. In model systems, where the fluid is at ambient temperature, one can visually observe the filtration processes by using plexiglass containers for the filter bed. In addition, due to the simplicity of construction of the apparatus, it is possible to arrange the experiment in such a way that samples of the filtered fluid can be obtained at any length throughout the filter bed, via syringe type ports along the filter depth.

Although a great deal of research has already been done on the depth filtration of solids suspended in water, the results cannot be reliably applied to the filtration of molten metals. This is because particles in water (a polar molecule) have a surface charge which is neutralized locally by counterions in the water, hence an electrical double layer is formed. Consequently, when double layers of approaching surfaces interact there are repulsive forces produced which may prevent entrapment[8]. On the other hand, molten metals being electrically conducting do not exhibit double layer repulsion phenomena thus a non-polar fluid is required for low temperature modeling.

For a variety of reasons (stability, toxicity, viscosity, ease of subsequent analysis, etc.) diesel fuel with $CaCo_3$ contaminants was chosen as the system for the model. The experimental apparatus is shown schematically in Figure 5, consisting of a plexiglas column 80cm in length and 5.65cm internal diameter, packed with tabular alumina particles to give a filter depth of 75cm. The tabular alumina size was varied during the experiments (0.1cm, 0.4cm and 0.8 cm in diameter) while the feed was kept constant by suspending a known amount of $CaCo_3$ (1 to 3μm diameter) in fixed diesel fuel of known and consistent quality to obtain a well mixed suspension of 30 ppm. The column was fitted with 10 sample ports along the filter height.

A constant experimental procedure was used throughout the study: the filter column and associated plumbing was first thoroughly cleaned by purging with a water surfactant mix, followed by water, air drying and then a final rinse with clean diesel fuel. The column was then packed with the required grade of tabular alumina while being vibrated so that settling, and hence a reproducible packing density, would result. The bed was given a high flow rate flush with clean diesel to remove any loose contaminants.

The known carbonate/diesel suspension was made up in the stainless steel surge tank and recycled by the pump for an extended period so that the system could homogenize, equilibrate and thermally stabilize. After this period, the suspension was allowed to flow into the filter at a known rate (measured by rotometer and volume per unit time measurements). When two residence times had elapsed sampling was commenced, care being taken to ensure that the bleed from the sampling port did not exceed 10% of the total flow rate and as an added safeguard, the samples were taken sequentially from top to bottom, i.e. downstream to upstream, also some fluid ($20cm^3$) was always "drained off" from each port prior to the actual sample being taken. The

reason for these precautions was that the steady state of the bed would not be unduly disturbed and so that any disruption caused would not be reflected in the samples. The samples were analyzed using a Hitachi-Perkins-Elmer 139 UV-VIS spectrophotometer which had been previously calibrated against known standards of the same suspension.

The results of this investigation are presented and discussed in section 6.3.

6. RESULTS AND DISCUSSION

6.1 Aluminum Filtration

The data obtained from experiments in the current phase of the work, along with the coding system and calculated parameters discussed in section 3, are presented in Tables I through III and graphically represented in Figures 6 to 17 For clarity of presentation this data will be suddivided into sections by bed configuration.

6.1.1 Two inch layer of 1/2 inch dia alumina balls

As described in the preceeding report (AMMRC TR-80-16) the initial work was performed using a combination bed of 10 inches of 3 to 4 mm tabular alumina sandwiched by 2 layers of 1/2 inch alumina balls at either end. In the original work it was considered (based on the available literature and industrial experience) that the two layers of balls would only reduce turbulence, prevent blockage of the orifice and would not play a significant part in the filtration process. A confirmatory experiment showed that this was not a realistic appraisal of the situation: a two inch layer of 1/2 inch balls having a 60% filtration efficiency at a moderate flow rate.

Although this may superficially appear to be a high efficiency, it whould be noted that this was only a short term experiment and that, of course, with their lower surface area to volume ratio, the large balls would saturate much more rapidly than the fine tabular alumina. Since, however, the majority of

the experiments in this investigation are short term in nature (see section 3) this effect had to be quantified; thus the following extra bed arrangements were selected specifically for this purpose.

i) 10 inches of 1/2 inch balls. This allowed the kinetics of the 1/2 ball medium to be characterized without the channeling that would inevitably occur in a 2 inch bed.

ii) 10 inches of 1-3mm tabular alumina supported by a graphite baffle to prevent orifice clogging. This permitted study of the tabular alumina in isolation.

iii) a combination of 2 inches 1/2 inch balls plus 10 inches of 1-3mm tabular alumina, plus another 2 inches of 1/2 inch balls. This arrangement allowed a virtually direct comparison with the initial work where the effect of the balls was thought negligible, but a different grade of tabular alumina (3-4mm) was used.

6.1.2 Ten inches of 1/2 inch diameter Alumina Balls

It can be seen from Figure 6 that the filtration efficiency of this bed decreased with increasing superficial melt velocity (flow rate). Figures 7 and 8 show the variation of K_o and Λ with flow rate, which in keeping with the initial work both show an increase with flow rate. An analysis of the K_o function (Figure 7) as described in section 3 shows it to be $0.006 + 0.028Um$. As can be seen from the graph, due to experimental constraints, the data is of such a nature that it would be unjustifiable to attribute any specific measure of precision to this calculated result. More low flow rate data would be required to obtain a meaningful determination of the tortuosity term (as given by the intercept), while the flow rate dependence term (as given by the slope) is probably not grossly in error. The calculated values are, however, adequate for comparison to the other bed configurations (see following sections), where it may be seen that flow rate dependence term is of the same order as that of the ten inch bed of tabular alumina. This correlation would be expected because although the grain size of the filter media is widely different, the porosity, ε, of the tabular and the balls (ε of 0.48 and 0.42 respectively) is

relatively constant, hence the flow geometry of the bed is similar. Figure 8 shows that Λ (the unit removal distance, where $\Lambda = 1/\lambda$, see section 3 and the preceeding report AMMRC TR-80-16) shows a marked increase with flow rate but appears to be reaching a finite value with further increases in flow rate.

6.1.3 10 inches of 1-3mm tabular alumina

In this configuration, the alumina balls used in the initial work were replaced by a graphite baffle to prevent orifice blockage; in this way the performance of the tabular medium could be studied in isolation. Figure 9 shows the variation in filtration efficiency with superficial melt velocity; it can be seen that the filtration efficiency starts at 99% and drops gradually with increasing flow rate. An analysis of the K_o function (Figure 10) yields $K_o = 0.008 + 0.036$ Um which shows approximatley the same flow rate dependency (slope) as the ten inches of 1/2 inch balls, but a higher tortuosity (intercept). Figure 11 shows Λ versus superficial flow rate, where it may be seen that Λ levels off at approximately 20 cm, after which it would appear to be insensitive to any further increases in flow rate. This behavior is in marked contrast to the 10 inches of 1/2 inch diameter balls where Λ varied significantly in the same range of flow rates; reaching a much larger limiting value at higher flow rates.

6.1.4 A combination bed of 2 inches of 1/2" balls plus 10 inches of 1-3mm tabular alumina plus 2 inches of 1/2" balls.

The above bed arrangement was chosen to allow direct comparison between the 4mm tabular alumina arrangement of the previous work with the 1-3mm used in the current series of results. The data resulting is shown in Figures 12, 13 and 14. It can be seen that in general the bed behaves in a manner very similar to the 10 inches of 1-3mm tabular alumina above. Analysis of the K_o function as $K_o = 0.003 + 0.059$ Um shows that the flow rate dependence is higher than in the tabular bed alone. The more significant comparison however, is

in the tortuosity term between this bed and the work performed on a similar combination bed of 4mm tabular alumina where $K_o = 0.0017 + 0.0131$ Um. It can be seen that the increase in tortuosity of the bed in the current work is reflected by about a doubling of the tortuosity term.

6.1.5 A 2 inch bed of 1-3mm tabular alumina.

The object of this series of experiments was twofold:

i) it would allow a direct comparison of the tabular alumina medium with the proposed work on a regular 2 inch thick Selee (open pore ceramic) filter.

ii) it shows whether the entire length of the 10 inch bed plays an equal part in filtration, or whether the top section has a disproportionately dominant role.

The results are presented in Figures 15 through 17 where it can be seen that the efficiency drops rapidly with flow rate. The analysis of the K_o function (Figure 16) reveals that $K_o = 0.014 + 0.111$Um, i.e. it shows that the flow rate dependence is very high, but also gives the impression of a high tortuosity value. This result is not as unexpected as it may at first appear: it indicates that the whole length of the longer beds is not utilized at all flow rates. This facet of the work is receiving further investigation, with particular reference to particle size distribution before and after filtration and the occurance of channeling. This superficially increased effectiveness of the shorter bed is reflected by the flow rate dependence of the unit distance Λ (Figure 17) which levels off at less than 10 Um.

6.1.6 A 2 inch bed of 1-3mm tabular alumina with reduced cross-sectional area.

The object of this section of the study was to characterize the clogging behavior of the tabular alumina bed medium. To accomplish this, a bed of considerably reduced capture volume was used. The melt to be filtered had a higher than normal TiB_2 content and several times the regular amount was passed through the filter. The melt flow was then arrested by freezing the whole filter unit. In this way the bed's arrangement, i.e. capture sites, particle distribution, etc. was preserved. The bed was then sectioned and is currently undergoing metallographic examination.

6.2 Steel Filtration

Table IV summarizes the successful scoping filtration experiments to date. In both runs Nos. 1 and 3, the Al_2O_3 was reduced approximately 7-fold (from 0.0784 to 0.0116 and 0.1945 to 0.0264, respectively). Whereas the total oxygen was reduced between 2 to 3 times in all three runs.

6.3 Low Temperature Model

The filtration efficiency as a function suspension velocity through this filter is shown in Figure 18 . The data clearly shows that as the velocity through the filter is increased the removal efficiency decreases. This reflects the trend observed in the molten metal filtration experiments, but it should be noted that the efficiency starts at a lower level and falls more rapidly with flow rate, than is the case in the molten metal system. The variation of $\ln \frac{C_i}{Co}$ as a function of filter distance through the packed bed is shown in Figure 4.

The parameters λ and K_o are plotted as a function of interstitial velocity in Figures 19 and 20. The parameter λ, steadily decreases with increasing velocity while the parameter K_o shows a slight increase with velocity followed by a slight decrease. Thus it can be seen that the kinetic parameter, K_o, is a very weak function of melt velocity. This may be illustrated by plotting K_o versus particle Reynolds number and comparing it to initial Al-TiB_2 work, as in Figure 21.

6.4 Summary

The work to date indicates that the filtration efficiency decreases with increasing melt velocity. The fundamental parameter K_o, which describes the particle capture kinetics has been shown to increase with melt velocity in all cases of aluminum filtration, but not in the hydrocarbon system.

The decrease in efficiency with flow rate would be expected from hydrodynamic forces acting within the filter bed; however this effect is tempered by the increase in K_o. An increase in K_o (the kinetic parameter) with melt velocity Um can be explained qualitatively from inclusion trajectory concept. Figure 22 shows fluid streamlines around a spherical filter grain. The limiting trajectory is one which just passes past the spherical filter grain at a distance of $\frac{d_i}{2}$, where d_i is the inclusion diameter. Here it is hypothesized that the primary mechanism of particle entrapment is interception by the filter grain. As one increases the fluid velocity across the filter grain, the inclusion having a higher mass inertia deviates from the fluid streamlines and tends to follow a path shown by a dotted line in Figure Also, as the fluid velocity increases, the number of inclusions which approach the filter grain also increases in proportion to the velocity. Since K is a measure of inclusion entrapment per unit time (see Eq. (1)), we find experimentally that K increases with melt velocity. However, at low Reynolds numbers, as was the case with the hydrocarbon system, the kinetic parameter is found to be a weak function of Reynold's number in the hydrocarbon-carbonate system because the inclusion inertia is low due to low fluid velocity.

Although the kinetic parameter increases with velocity, U_m, the filtration efficiency decreases. The filtration efficiency can be given by

$$\eta = \frac{C_i - C_o}{C_i} = 1 - e^{\frac{-K_o L}{U_m}} \qquad (14)$$

It is seen from the above that the ratio of kinetic parameter to melt velocity determines the efficiency of filtration. The ratio, K_o/U_m is defined as the filtration coefficient. That is

$$\eta = 1 - e^{-\lambda L} \qquad (15)$$

We note from the above equation that as the filtration coefficient, λ, increases the filtration efficiency will increase for a given filter length.

Although the kinetic parameter, K_o, increases with the melt velocity, U_m, as given in Figure 21, the filtration coefficient, λ, decreases, and is illustrated in Figure 23 for the Al-TiB_2 system.

It is noted that higher filtration efficiencies are obtained at lower melt velocities (Figure 9). However, if one is constrained by high melt velocities due to production requirements, higher inclusion removal can also be obtained by increasing the filter length.

7. FUTURE WORK

Work is planned in several different areas:

7.1 Aluminum Filtration

- Evaluation of open pore ceramic filters and other filtration media.
- Evaluation of depth filtration will continue, with particular reference to the hydrodynamic aspects of the industrial practice of introducing a counter-current gas flow.

7.2 Steel Filtration

- Evaluate filtration efficiency initially using Al_2O_3 tabular beds.

7.3 Superalloy Filtration

- Evaluation of filtration efficiency initally using Al_2O_3 tabular beds. Work is currently in progress to design modifications to the steel filtration apparatus for super alloy work.

7.4 Low Temperature Modeling

- After the completion of the diesel/calcium carbonate experiments which represented solid inclusions in liquid metal systems, a model is now being considered for liquid inclusions. Liquid inclusions are present in steel melts and in aluminum after chlorine gas treatment. A model flow system consisting of ditoluyl inclusions in water passing through a filter of glass (spherical) packing is now in its conceptual stages.

- The independent variables in this experimental program would be suspension velocity, filter grain size and filter grain type. The dependent variables being inclusion concentration and size distribution along the filter bed. In tandem with the experimental program the system could be math modeled to better understand the effect of the process variables.
- This work may be extended to include a flow visualization study which will pictorially record and illustrate the capture, saturation and subsequent release phenomena of liquid inclusions in packed beds.

7.5 Mathematical Modeling of Inclusion Flow Trajectory in an Accelerated Flow Field

Flow of melts containing inclusions through a packed bed can be visualized at a macroscopic level as given below:

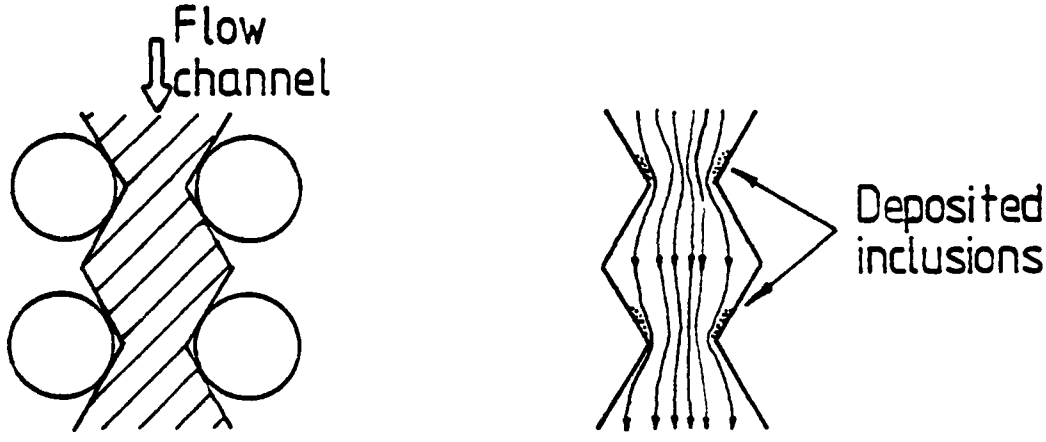

Figure 24.

- Work is underway to describe particle trajectory as it flows through an idealized, but an existing, flow geometry as shown in Figure 24. Since the cross sectional area available for flow decreases, and then increases periodically, the particle and the melt become accelerated and decelerated repeatedly, as they flow through the bed. Since the inclusion has a higher inertia, it does not follow the same path as the fluid and tends to accumulate in the

shaded areas shown. Theoretical modeling of the melt flow behavior and the particle trajectory is being taken up at the present moment.

REFERENCES

1. British Patent 1,148,344, Foseco International Limited, G. Snow, 1969.

2. A. Buckley: Giesserei, 1961, vol. 51, pp. 655-659.

3. F. R. Mollard, N. Davidson: "Ceramic Foam - A Unique Method of Filtering Molten Aluminum in the Foundry" - presented at the 1978 AFS Conference, Detroit, Michigan.

4. K. J. Brondyke, P. D. Hess: Trans. TMS-AIME, 1964, vol. 230, pp. 1553-1556.

5. M. V. Brant, D. C. Bone and E. F. Emley: Metall. Soc. AIME, TMS paper No. A70-51.

6. D. Apelian, R. Mutharasan and R. O'Malley: "Depth Filtration of Liquid Metals: Part I - Theoretical, submitted to Trans. AIME, 1980.

7. A. McLean: Journal of Metals, March 1968, Vol. 20, No. 3, pp. 96-100.

8. Spielman, L. A.: "Particle Capture from Low-Speed Laminar Flows", Ann. Rev. Fluid Mech. Vol. 9, p. 297, 1977.

Table I: Filter Bed Data

sample	d(in)	bed arrangement[1]	particle size[2]	bed diameter
DT101	.043	2"B-10"T-2"B	d_p=1-2mm, d_B=2cm	3"
DT102	.043	"	"	"
DT201	.059	"	"	"
DT202	.059	"	"	"
DT301	.073	"	"	"
DT302	.073	"	"	"
DT401	.106	"	"	"
DT402	.106	"	"	"
DT403	.106	"	"	"
DT501	.147	"	"	"
DT502	.147	"	"	"
DT503	.147	"	"	"
DT601	.173	"	"	"
DT602	.173	"	"	"
DT603	.173	"	"	"
DT701	.147	"	"	"
DT702	.147	"	"	"
DT703	.147	"	"	"
DT801	.094	"	"	"
DT802	.094	"	"	"
DT803	.094	"	"	"
DT901	.122	"	"	"
DT902	.122	"	"	"
DT903	.122	"	"	"

Table I - continued

sample	d(in)	bed arrangement[1]	particle size[2]	bed diameter
DT1001	.097	2"B-2"T-2"B	d_p=1-2mm, d_B=2cm	3"
DT1002	.097	"	"	"
DT1101	.148	"	"	"
DT1102	.148	"	"	"
DT1201	.148	2"B	d_B=2cm	"
DT1202	.148	"	"	"
DT1301	.096	2"T	d_p=3mm	1 3/8"
DT1302	.096	"	"	"
DT1303	.096	"	"	"
DT1304	.096	"	"	"
DT1305	.096	"	"	"
DT1306	.096	"	"	"
DT1307	.096	"	"	"
DT1401	.059	10"T	"	3"
DT1402	.059	"	"	"
DT1403	.059	"	"	"
DT1501	.082	"	"	"
DT1502	.082	"	"	"
DT1503	.082	"	"	"
DT1504	.082	"	"	"
DT1601	.116	"	"	"
DT1602	.116	"	"	"
DT1603	.116	"	"	"
DT1701	.166	"	"	"
DT1702	.166	"	"	"
DT1703	.166	"	"	"

Table I - continued

sample	d(in)	bed arrangement[1]	particle size[2]	bed diameter
DT1801	.07	2"T	d_p=3mm	4"
DT1802	.07	"	"	"
DT1803	.07	"	"	"
DT1804	.07	"	"	"
DT1901	.110	"	"	"
DT1902	.110	"	"	"
DT1903	.110	"	"	"
DT1904	.110	"	"	"
DT2001	.150	"	"	"
DT2002	.150	"	"	"
DT2003	.150	"	"	"
DT2101	.200	"	"	"
DT2102	.200	"	"	"
DT2103	.200	"	"	"
DT2201	.220	"	"	"
DT2202	.220	"	"	"
DT2203	.220	"	"	"
DT2301	.073	10"B	d_B=2cm	"
DT2501	.152	"	"	"
DT2502	.152	"	"	"
DT2503	.152	"	"	"
DT2504	.152	"	"	"

Table I - continued

sample	d(in)	bed arrangement[1]	particle size[2]	bed diameter
DT2701	.221	10"B	d_B=2cm	4"
DT2702	.221	"	"	"
DT2703	.221	"	"	"

1. B = layer of balls, T = layer of tabs

2. d_p= diameter of particle, d_B= diameter of ball

TABLE II - Flow Rate Data

Sample	Q(cm^3/sec)	FF (lb/hr-in^2)	Um(cm/sec)	Um^{-1}(sec/cm)
DT101	1.36	3.53	0.03	33.33
DT102	1.36	3.53	0.030	33.33
DT201	*	*	*	*
DT202	*	*	*	*
DT301**	1.82	4.91	0.040	25.0
DT302**	1.82	4.91	0.040	25.0
DT401	1.39	3.61	0.030	33.33
DT402	2.93	7.63	0.064	15.63
DT403	1.74	4.52	0.038	26.32
DT501	3.69	9.58	0.081	12.38
DT502	3.54	9.22	0.078	12.82
DT503	3.54	9.22	0.078	12.82
DT601	28.82	74.96	0.632	1.58
DT602	32.11	83.51	0.704	1.42
DT603	32.11	83.51	0.704	1.42
DT701	27.52	71.58	0.604	1.66
DT702	25.06	65.17	0.550	1.82
DT703	24.28	63.15	0.532	1.88
DT801	6.23	16.80	0.137	7.30
D802	6.74	18.13	0.148	6.70
DT803	5.16	13.88	0.113	8.85
DT901	13.95	37.56	0.306	3.27
DT902	13.16	35.43	0.289	3.46
DT903	13.65	36.74	0.299	3.34
DT1001	8.84	23.80	0.194	5.15
DT1002	10.16	27.34	0.223	4.48
DT1101	22.43	60.36	0.492	2.03

Table II - continued

Sample	$Q(cm^3/sec)$	$FF(lb/hr\text{-}in^2)$	Um(cm/sec)	$Um^{-1}(sec/cm)$
DT1102	22.16	59.65	0.486	2.06
DT1201	13.65	36.74	0.299	3.34
DT1202	12.64	34.01	0.277	3.61
DT1301	9.70	124.00	1.016	0.98
DT1302	10.12	129.30	1.056	0.95
DT1303	3.46	44.20	0.361	2.77
DT1304	7.10	90.30	0.741	1.35
DT1305	7.29	93.00	0.761	1.31
DT1306	5.61	71.70	0.586	1.71
DT1307	4.66	59.53	0.486	2.06
DT1401	3.70	9.95	0.082	12.20
DT1402	3.51	9.44	0.078	12.82
DT1403	3.63	9.77	0.081	12.34
DT1501	2.70	7.26	0.060	16.66
DT1502	2.66	7.16	0.059	16.95
DT1503	2.57	6.93	0.057	17.54
DT1504	2.66	7.17	0.059	16.95
DT1601	15.81	42.56	0.347	2.88
DT1602	15.13	40.74	0.336	2.98
DT1603	14.92	40.14	0.331	3.02
DT1701	26.77	72.06	0.594	1.68
DT1702	34.55	93.02	0.766	1.31
DT1703	31.44	84.63	0.697	1.43
DT1801	8.30	12.57	0.102	9.80
DT1802	8.49	12.85	0.104	9.62
DT1803	7.51	11.36	0.093	10.80
DT1804	9.08	13.75	0.112	8.93

Table II - continued

Sample	Q(cm^3/sec)	FF(lb/hr-in^2)	Um(cm/sec)	Um^{-1}(sec/cm)
DT1901	8.29	12.56	0.102	9.80
DT1902	10.70	16.20	0.132	7.58
DT1903	12.56	19.01	0.156	6.45
DT1904	7.22	10.94	0.089	11.24
DT2001	21.58	32.67	0.266	3.76
DT2002	19.20	29.09	0.237	4.22
DT2003	17.66	26.73	0.218	4.59
DT2101	40.10	60.68	0.495	2.18
DT2102	37.95	57.45	0.468	2.14
DT2103	36.98	55.99	0.456	2.19
DT2201	45.11	68.29	0.556	1.80
DT2202	39.25	59.43	0.484	2.07
DT2203	25.54	38.66	0.315	3.17
DT2301	8.20	12.38	0.101	9.90
DT2501	23.93	64.40	0.295	3.39
DT2502	23.07	62.10	0.285	3.51
DT2503	22.24	59.86	0.274	3.65
DT2504	12.06	32.46	0.149	6.71
DT2701	55.42	149.16	0.683	1.46
DT2702	58.51	157.49	0.722	1.39
DT2703	27.89	75.06	0.344	2.91

* - no data available

** - data estimated

Table III - Filtration Data

sample	Ci(ppm TiB_2)	Co(ppm TiB_2)	ln Ci/Co	η	Ko(sec^{-1})	λ(cm^{-1})	Λ(cm)
DT1I	505						
DT101	505	15	3.52	.97	.0042	.139	7.19
DT102	505	15	3.52	.97	.0042	.139	7.19
DT2I	1377						
DT201	1377	15	4.52	.99	---	---	---
DT202	1377	15	4.52	.99	---	---	---
DT3I	245						
DT301	245	15	2.80	.94	.0044	.110	9.09
DT302	245	15	2.80	.94	.0044	.110	9.09
DT4I	176						
DT401	176	15	2.46	.91	.0029	.097	10.34
DT402	176	15	2.46	.91	.0062	.097	10.31
DT403	176	15	2.46	.91	.0037	.097	10.31
DT5I	69						
DT501	69	15	1.53	.78	.0048	.060	16.67
DT502	69	15	1.53	.78	.0048	.060	16.67
DT503	69	15	1.53	.78	.0048	.060	16.67
DT6I	819						
DT601	819	100	2.10	.88	.0523	.083	12.04
DT602	819	214	1.34	.74	.0371	.053	18.80
DT603	819	222	1.31	.73	.0363	.052	19.39
DT7I	757						
DT701	757	69	2.40	.91	.0570	.095	10.60
DT702	757	153	1.60	.80	.0346	.063	15.87
DT703	757	214	1.26	.72	.0264	.050	20.08

Table III - Filtration Data (continued)

sample	Ci(ppm TiB_2)	Co(ppm TiB_2)	ln Ci/Co	η	Ko(sec^{-1})	λ(cm^{-1})	Λ(cm)
DT8I	458						
DT801	458	17	3.29	.96	.0178	.130	7.70
DT802	458	15	3.42	.97	.0198	.135	7.41
DT803	458	89	1.64	.81	.0073	.065	15.48
DT9I	817						
DT901	817	18	3.80	.98	.0458	.150	6.68
DT902	817	23	3.57	.97	.0410	.142	7.09
DT903	817	23	3.57	.97	.0424	.142	7.09
DT10I	939						
DT1001	939	575	0.49	.39	.0037	.019	51.81
DT1002	939	253	1.31	.74	.0115	.052	19.23
DT11I	791						
DT1101	791	190	1.43	.76	.1381	.281	3.56
DT1102	791	311	0.93	.61	.0893	.184	5.44
DT12I	705						
DT1201	705	283	0.91	.60			
DT1202	705	291	0.89	.59			
DT13I1	880						
DT13I2	1683						
DT13I3	2448						
DT13I4	750						
DT13I5	1025						
DT1301	880	849	0.036	.04	.0072	.007	141.65
DT1302	880	406	0.774	.54	.1608	.152	6.57

Table III - Filtration Data (continued)

sample	Ci(ppm TiB_2)	Co(ppm TiB_2)	ln Ci/Co	η	Ko(sec^{-1})	λ(cm^{-1})	Λ(cm)
DT1303	1683	15	4.72	.99	.3350	.929	1.08
DT1304	2448	589	1.42	.76	.2078	.280	3.56
DT1305	2448	84	3.37	.97	.5052	.664	1.51
DT1306	750	559	0.29	.26	.0339	.058	17.28
DT1307	1025	291	1.26	.71	.1205	.248	4.03
DT14I1	1094						
DT14I2	1300						
DT1401	1094	23	3.86	.98	.0125	.152	6.58
DT1402	1094	31	3.56	.97	.0109	.140	7.14
DT1403	1300	31	3.74	.98	.0119	.147	6.80
DT15I1	1056						
DT15I2	834						
DT15I3	3060						
DT1501	1056	23	3.83	.98	.0090	.151	6.63
DT1502	834	46	2.90	.94	.0067	.114	8.76
DT1503	3060	31	4.60	.99	.0103	.181	5.52
DT1504	3060	23	4.89	.99	.0114	.193	5.19
DT16I1	1285						
DT1601	1285	168	2.04	.87	.0279	.080	12.50
DT1602	1285	199	1.87	.85	.0247	.074	13.51
DT1603	1285	482	0.98	.63	.0128	.039	25.64
DT17I1	2601						
DT1701	2601	887	1.08	.66	.0253	.043	23.26
DT1702	2601	872	1.09	.67	.0329	.043	23.26
DT1703	2601	673	1.35	.74	.0370	.053	18.87

Table III - Filtration Data (continued)

sample	Ci(ppm TiB_2)	Co(ppm TiB_2)	ln Ci/Co	n	Ko(sec^{-1})	λ(cm^{-1})	Λ(cm)
DT18I1	2295						
DT1801	2295	413	1.72	.82	.0344	.338	2.96
DT1802	2295	182	2.53	.92	.0519	.499	2.00
DT1803	2295	199	2.45	.91	.0448	.481	2.07
DT1804	2295	118	2.97	.95	.0654	.584	1.71
DT19I1	101						
DT19I2	364						
DT1901	364	---	---	---	---	---	---
DT1902	364	222	0.49	.39	.0128	.097	10.31
DT1903	364	144	0.93	.60	.0285	.183	5.45
DT1904	364	96	1.33	.74	.0234	.262	3.82
DT20I1	2601						
DT20I2	1989						
DT2001	2601	640	1.40	.75	.0734	.276	3.62
DT2002							
DT2003	1989	692	1.06	.65	.0453	.208	4.80
DT21I1	3366						
DT21I2	1989						
DT2102	3366	1989	0.53	.41	.0485	.104	9.61
DT2103	1989	918	0.77	.54	.0694	.152	6.58
DT22I1	7344						
DT22I2	2907						
DT2201	7344	3366	0.78	.54	.0854	.154	6.49
DT2202	7344	3978	0.61	.46	.0584	.121	8.26
DT2203	7344	3519	0.74	.52	.0456	.145	6.90

Table III - Filtration Data (continued)

sample	Ci(ppm TiB_2)	Co (ppm TiB_2)	ln Ci/Co	η	Ko(sec^{-1})	λ(cm^{-1})	Λ(cm)
DT23I1	1836						
DT23I2	421						
DT2301	1836	337	1.70	.82	.0068	.067	15.00
DT25I1	1530						
DT25I2	499						
DT2501	1530	745	0.72	.51	.0084	.028	35.20
DT2502	1530	413	1.31	.73	.0147	.052	19.40
DT2503	1530	266	1.75	.83	.0189	.069	14.50
DT2504	499	155	1.17	.69	.0069	.046	21.70
DT27I1	822						
DT27I2	2142						
DT2 701	822	439	0.63	.47	.0169	.025	40.30
DT2702	2142	722	1.09	.66	.0309	.043	23.30
DT2703	2142	393	1.70	.82	.0230	.067	14.90

TABLE IV

Summary of Filtration Experiments

	Wt % Al_2O_3		Wt % Oxygen	
Run No.	inlet to filter	outlet	inlet to filter	outlet
1	0.0784	0.0116	0.0365	0.0114
2	0.2644	0.0019	0.18	0.10
3	0.1945	0.0264	0.17	0.06

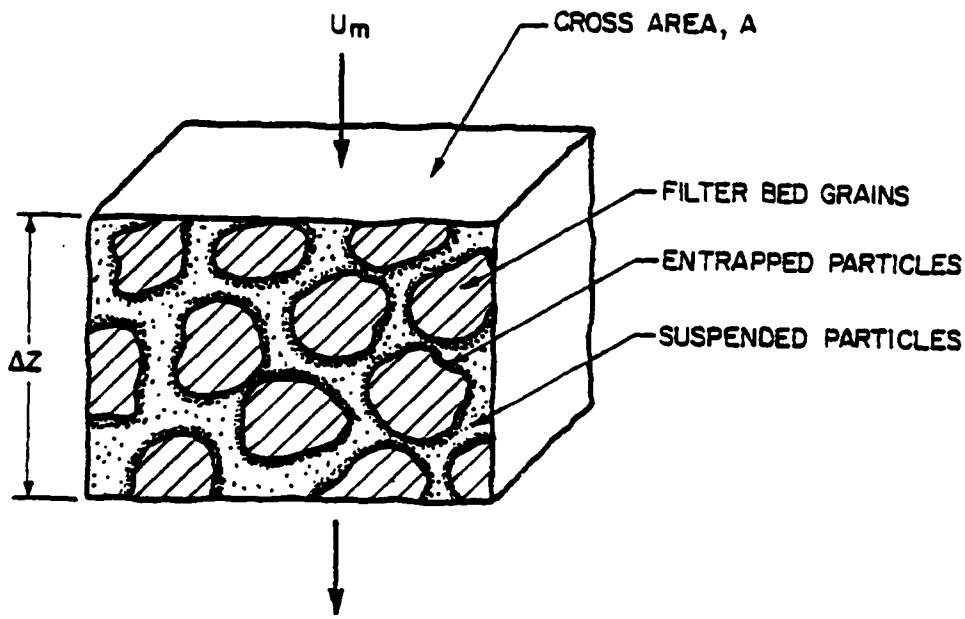

Figure 1. Differential cross-section of Depth Filter.

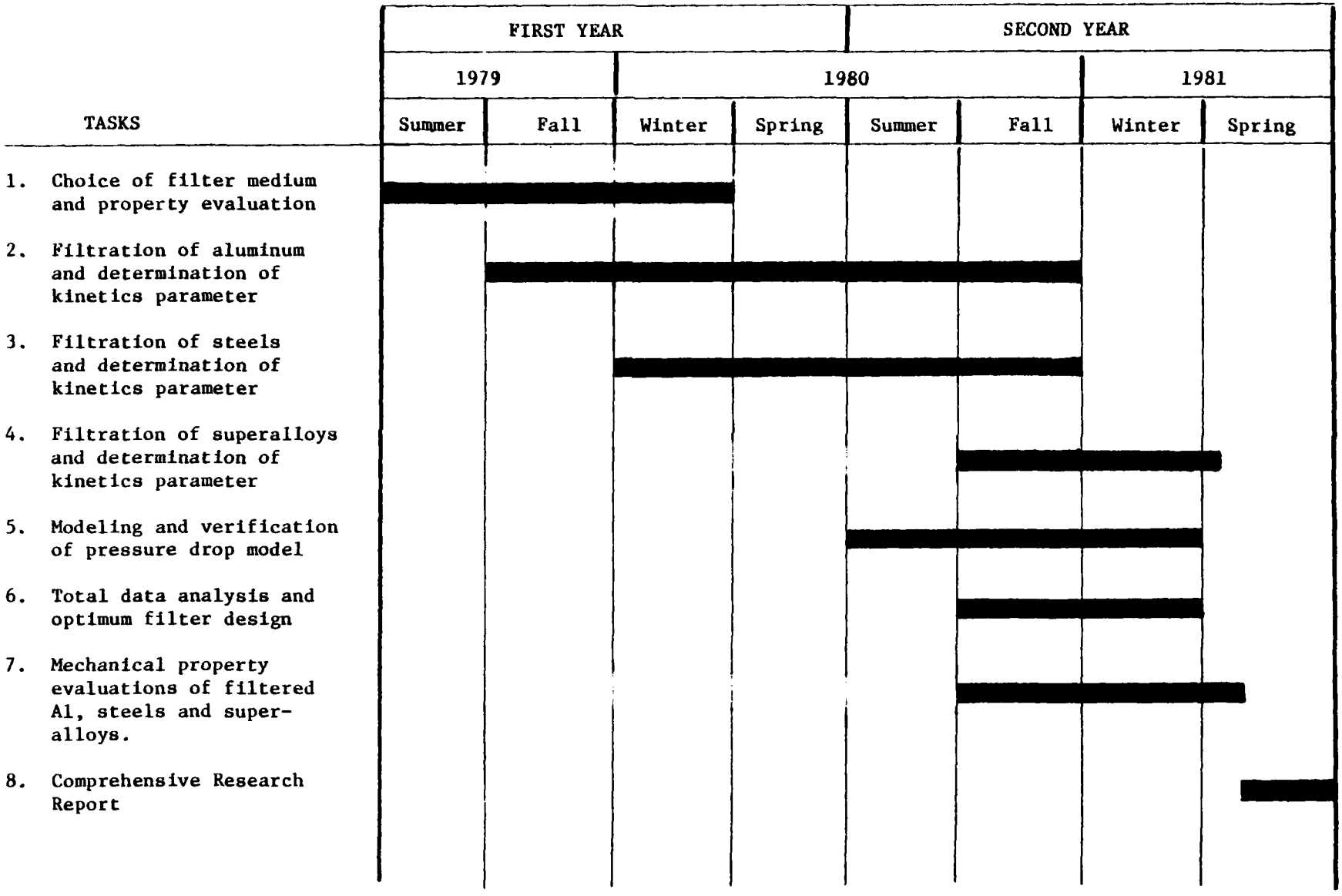

Figure 2. Proposed Program Schedule

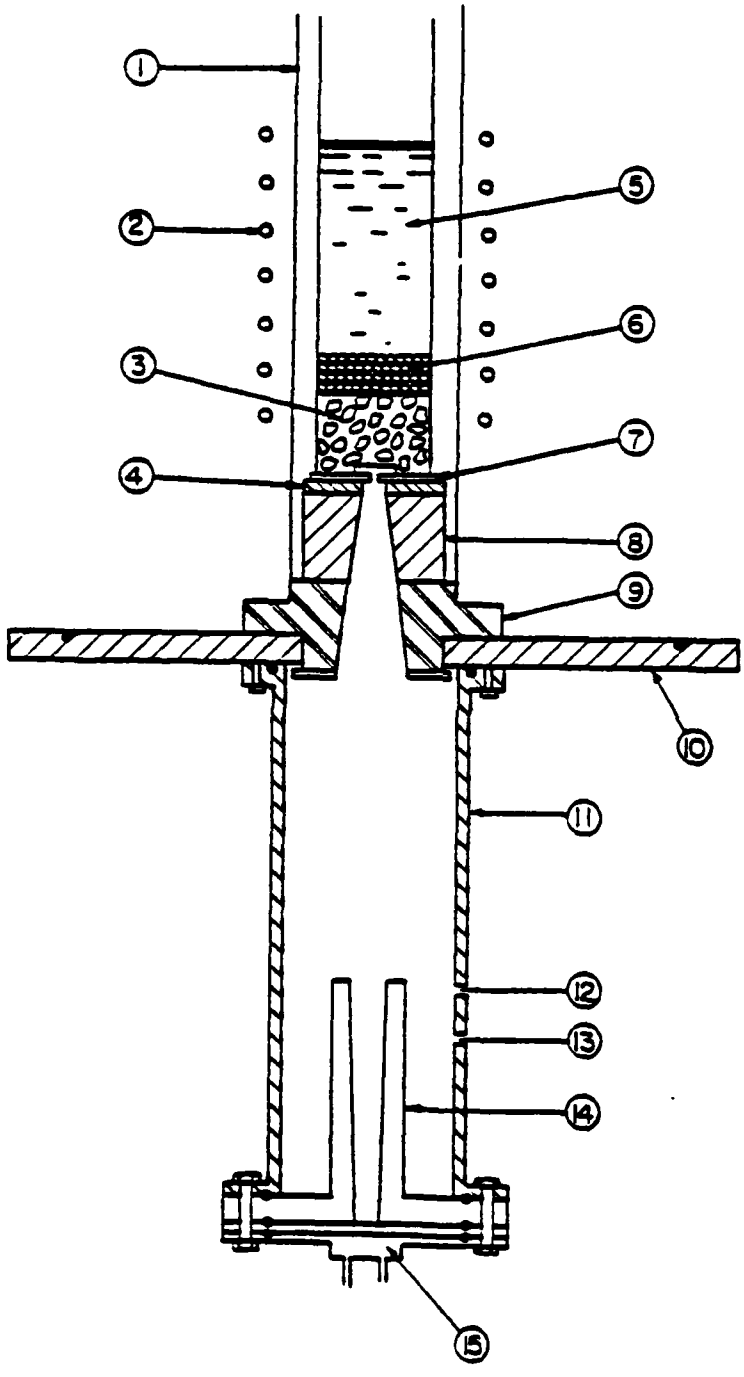

Legend

1. Graphite susceptor
2. Induction coil
3. Filter bed
4. Al_2O_3 disc
5. Steel melt
6. Particle valve
7. Orifice disc
8. Pyrolitic graphite
9. Stainless steel pedestal
10. Base plate supporting don
11. Lower chamber
12. Vacuum fittings
13. T/C fittings
14. Mold
15. Chill

Figure 3. Schematic diagram of steel filtration apparatus.

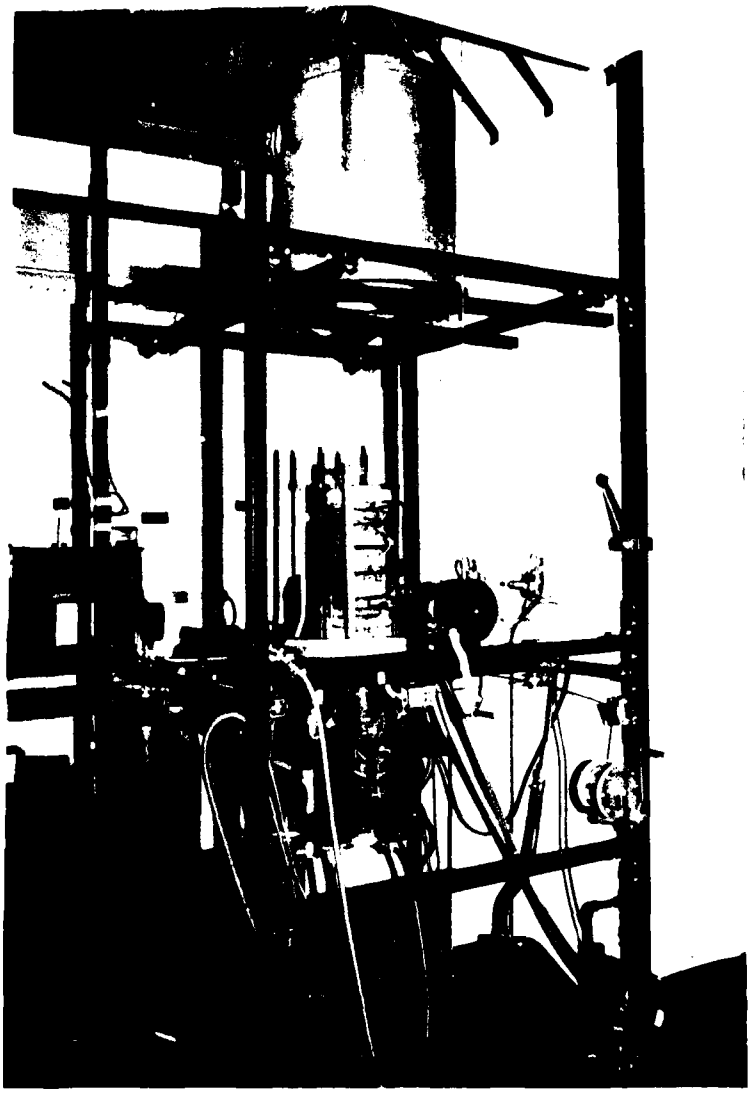

Figure 4. Photograph of Steel Filtration Apparatus

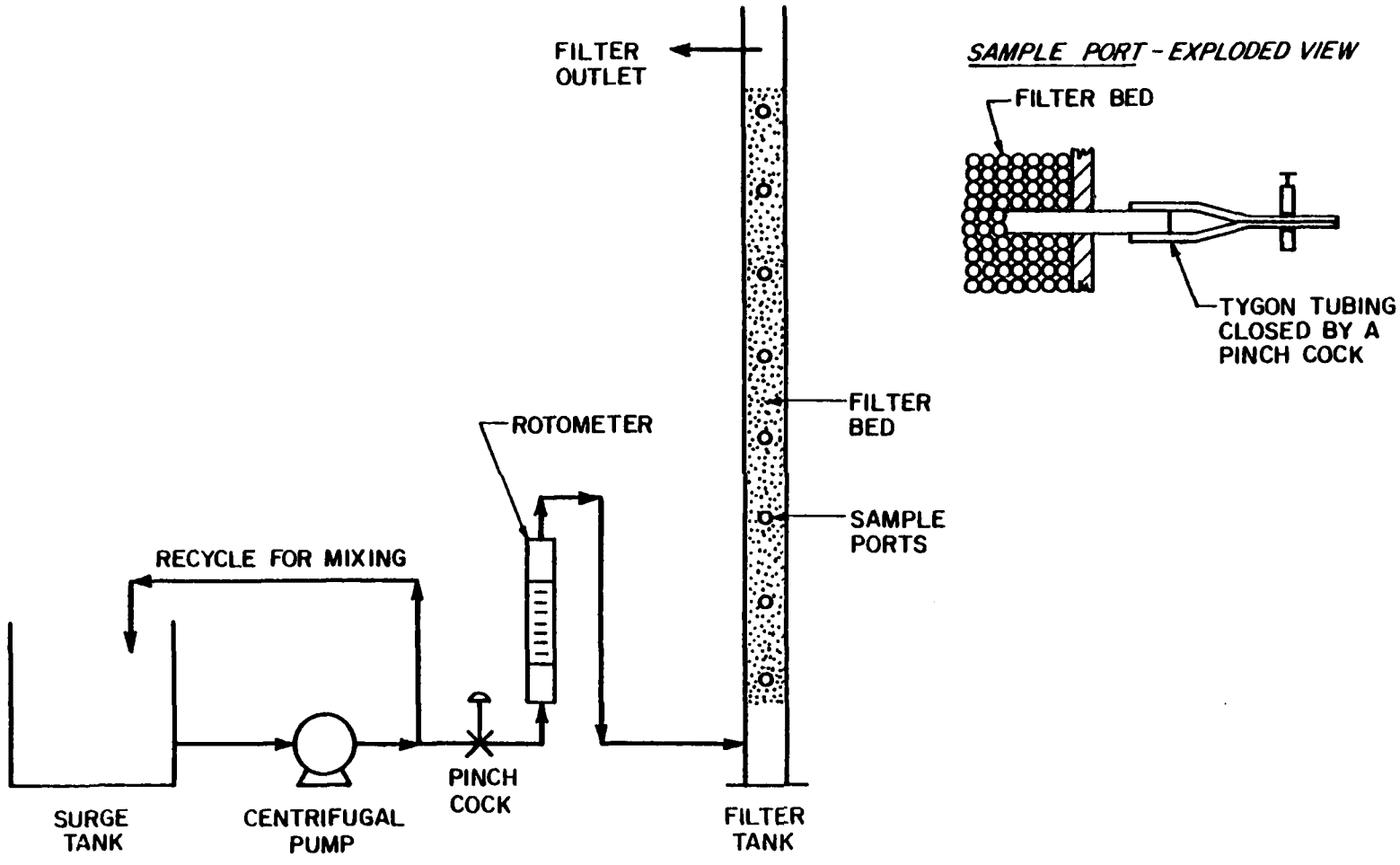

Figure 5. Schematic of Low Temperature Model Apparatus.

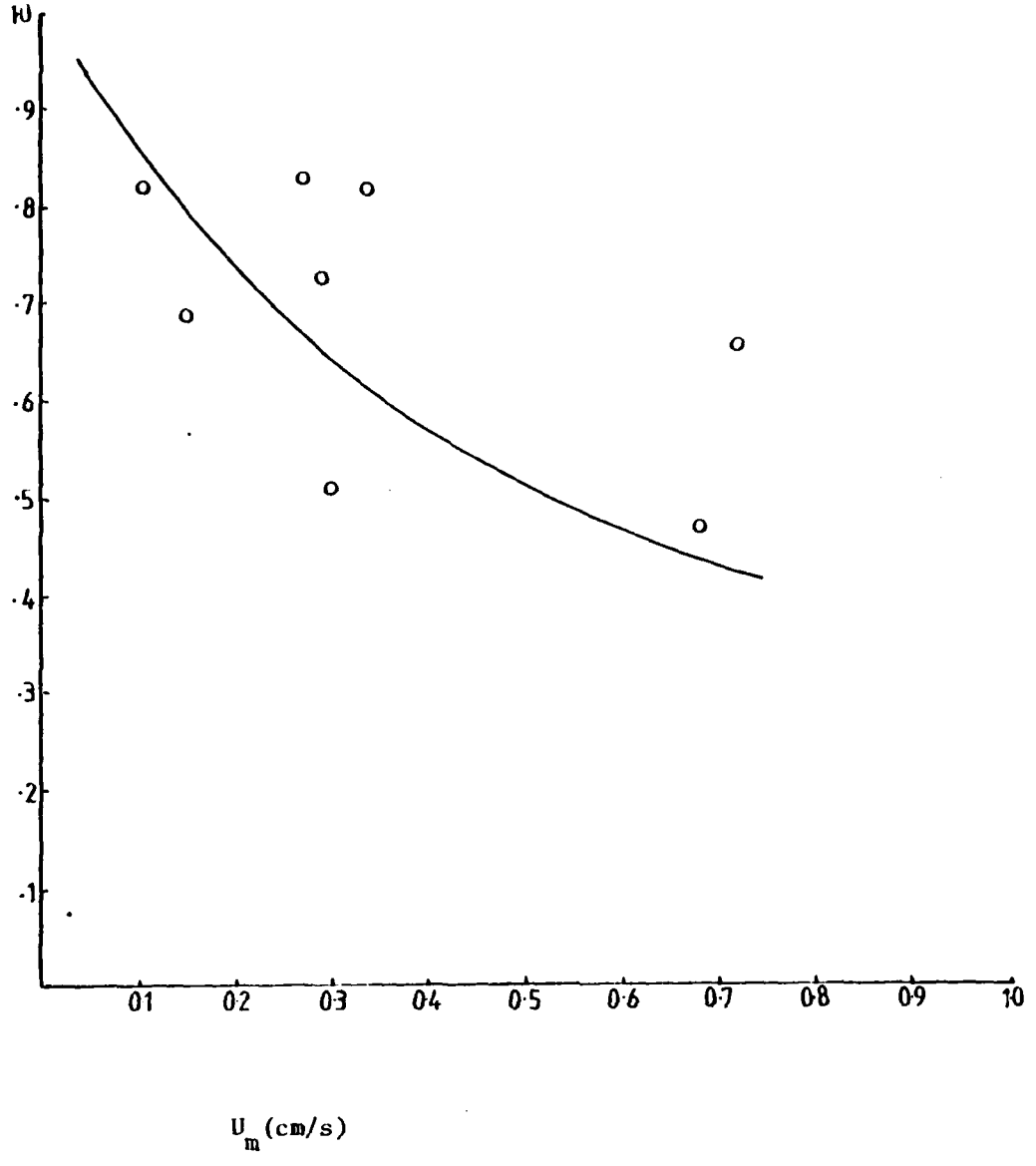

Figure 6. The variation in filtration efficiency with superficial melt velocity for a 10" bed of 1/2" balls.

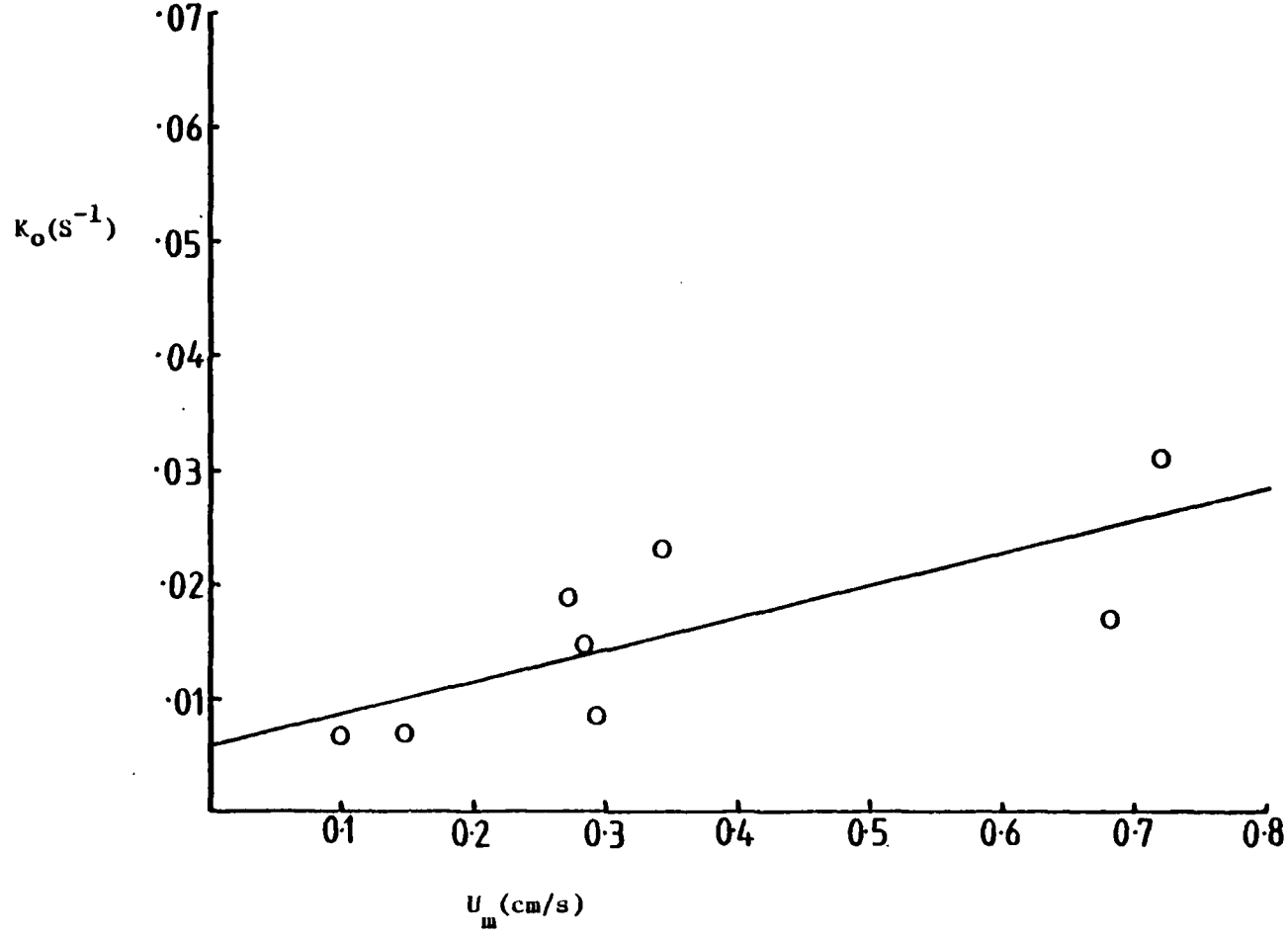

Figure 7. The variation of K_o with superficial melt velocity for a 10" bed of 1/2" balls.

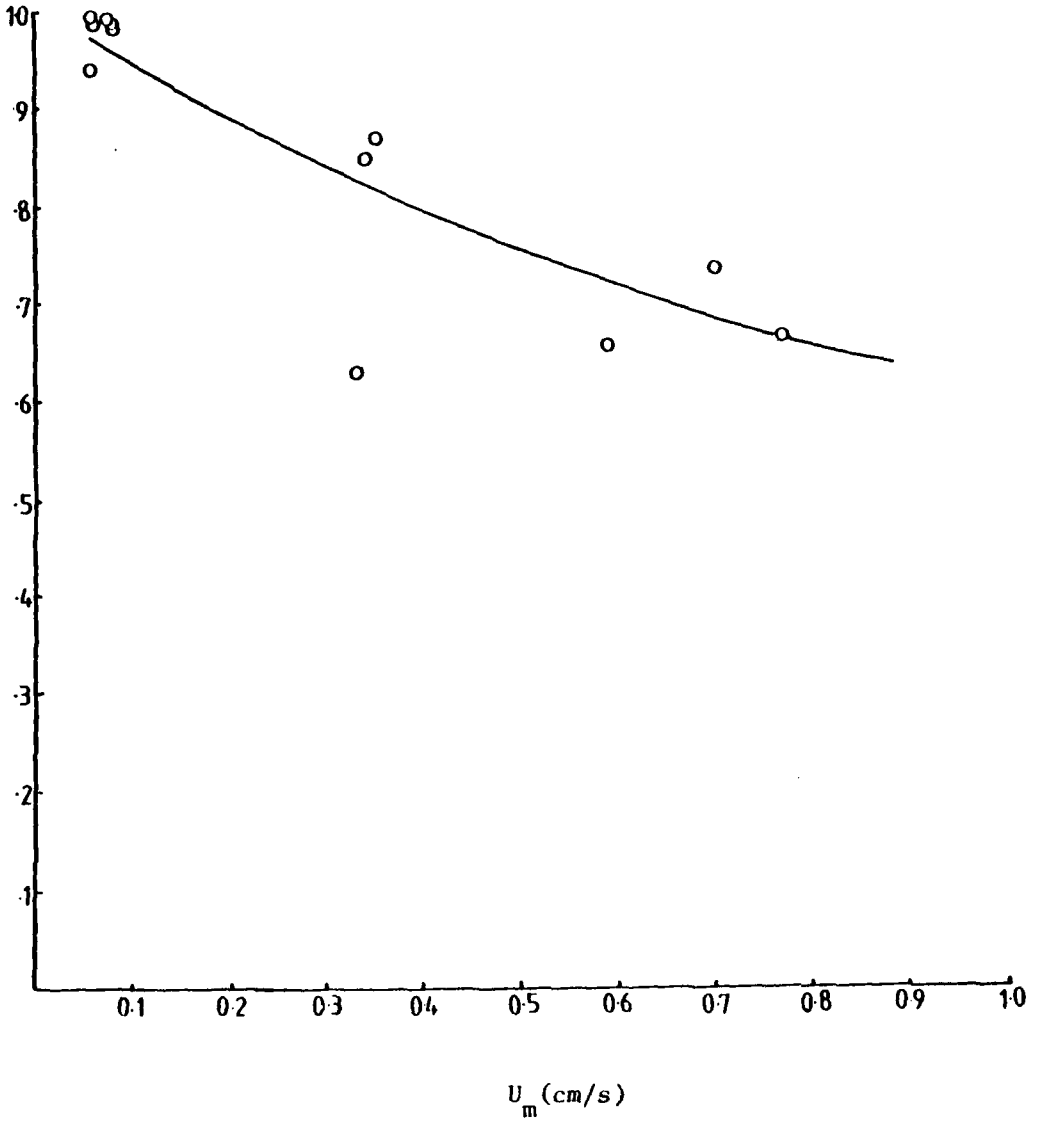

Figure 9. The variation in filtration efficiency with superficial melt velocity for a 10" bed of 1-3mm tabular alumina.

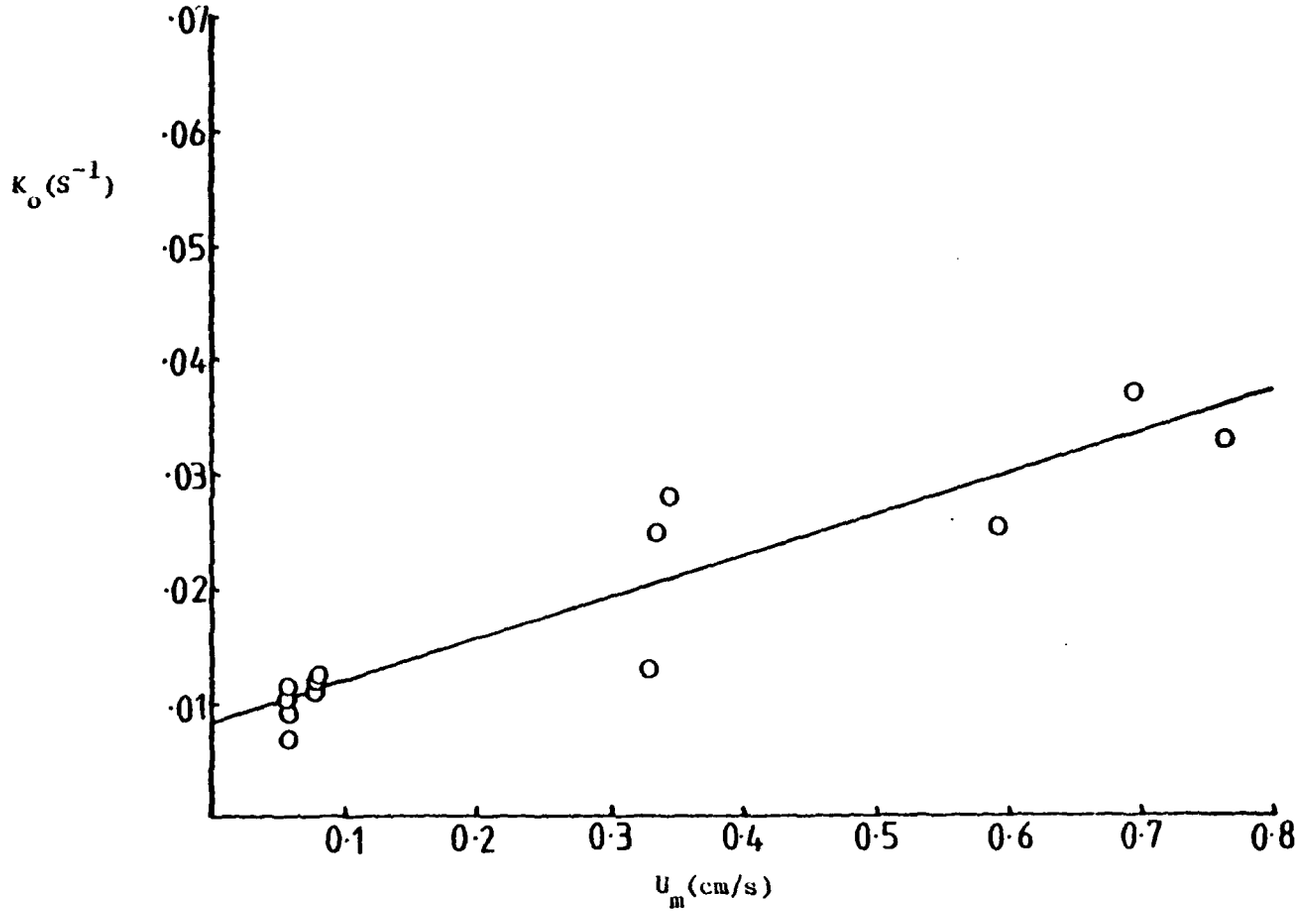

Figure 10. The variation of K_o with superficial melt velocity for a 10" bed of 1-3mm tabular alumina.

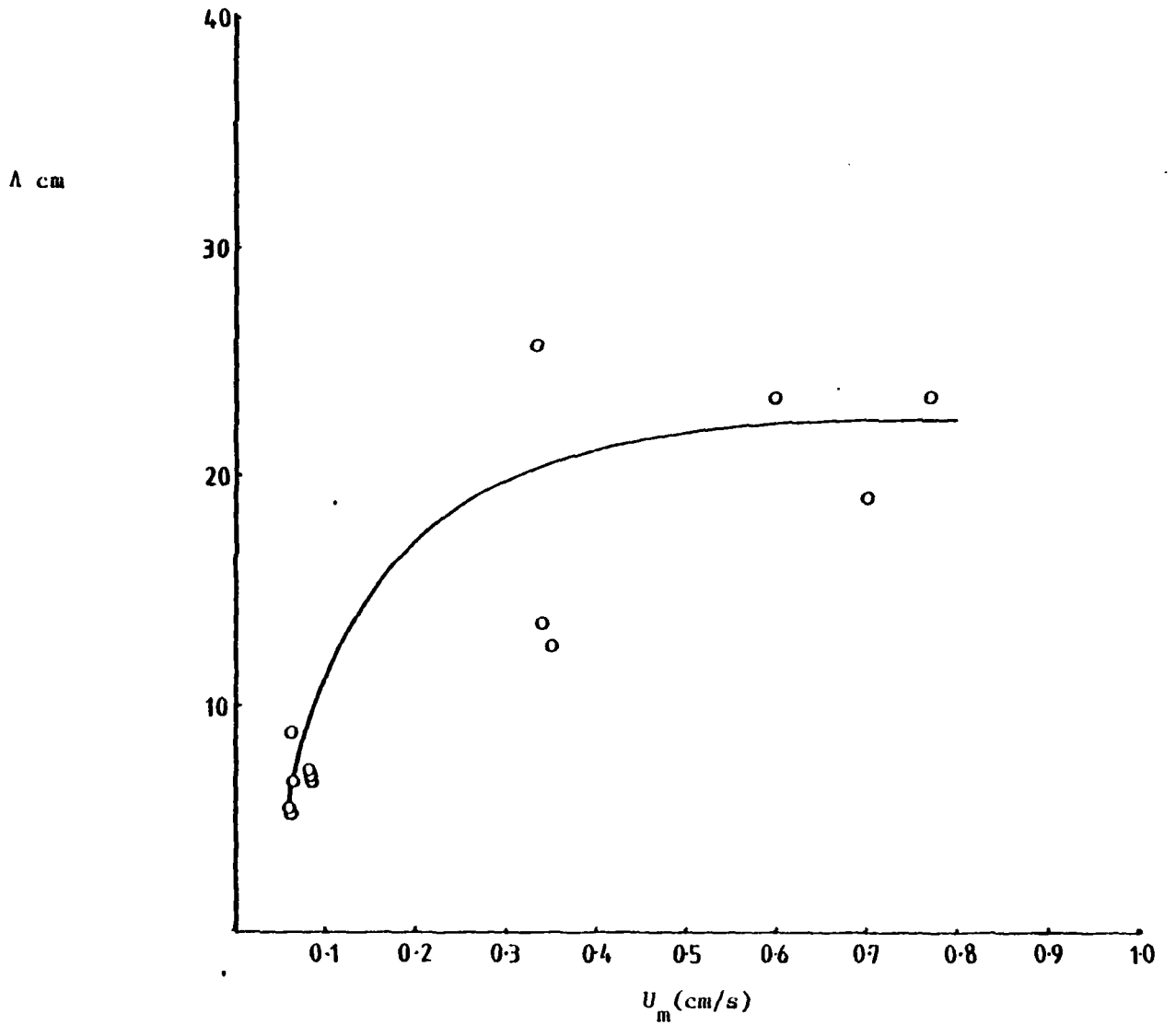

Figure 11. The variation of Λ with superficial melt velocity for a 10" bed of 1-3mm. tabular alumina.

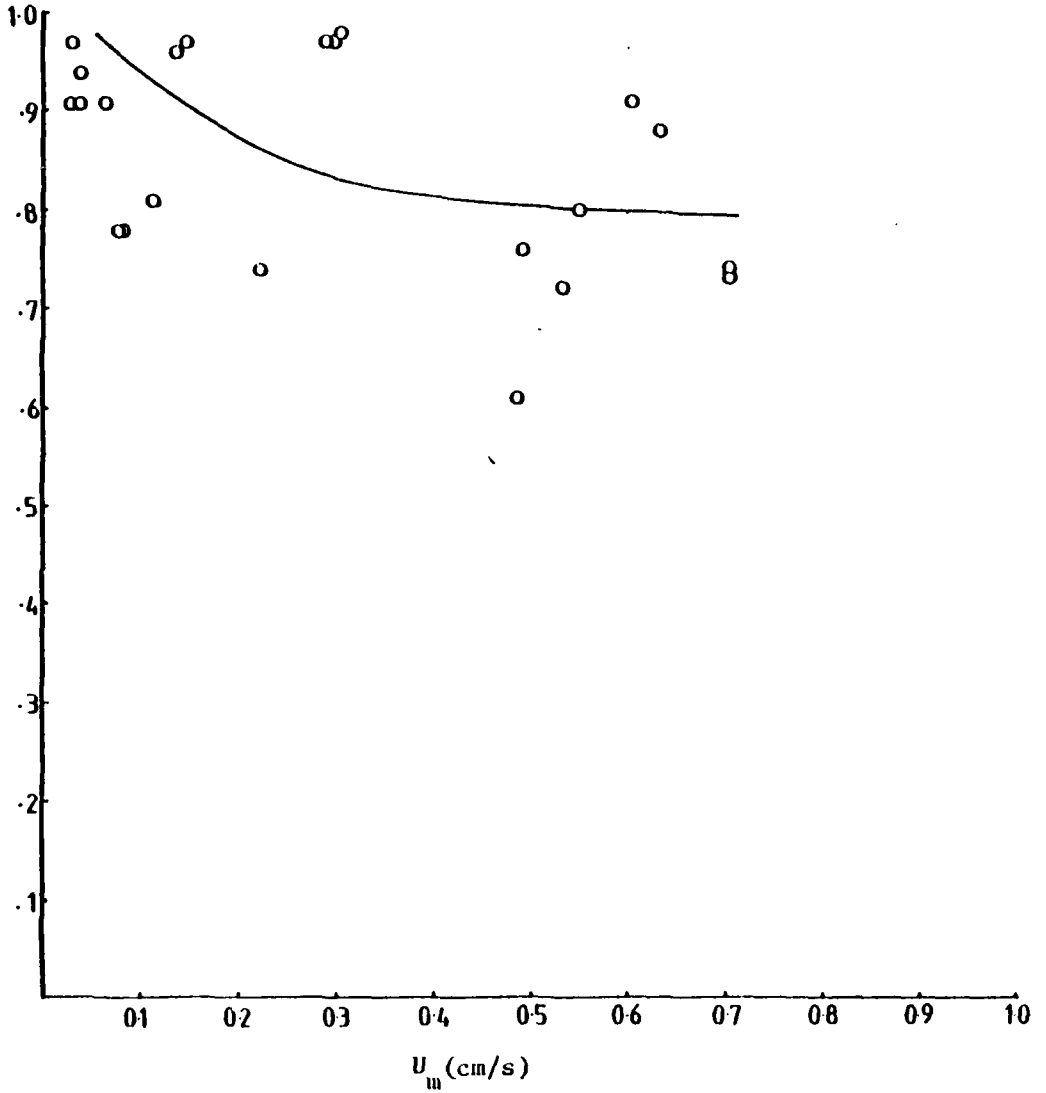

Figure 12. The variation in filtration efficiency with superficial melt velocity for a sandwich bed arrangement of 2" of 1/2" balls plus 10" of 1-3mm tabular alumina plus 2" of 1/2" balls.

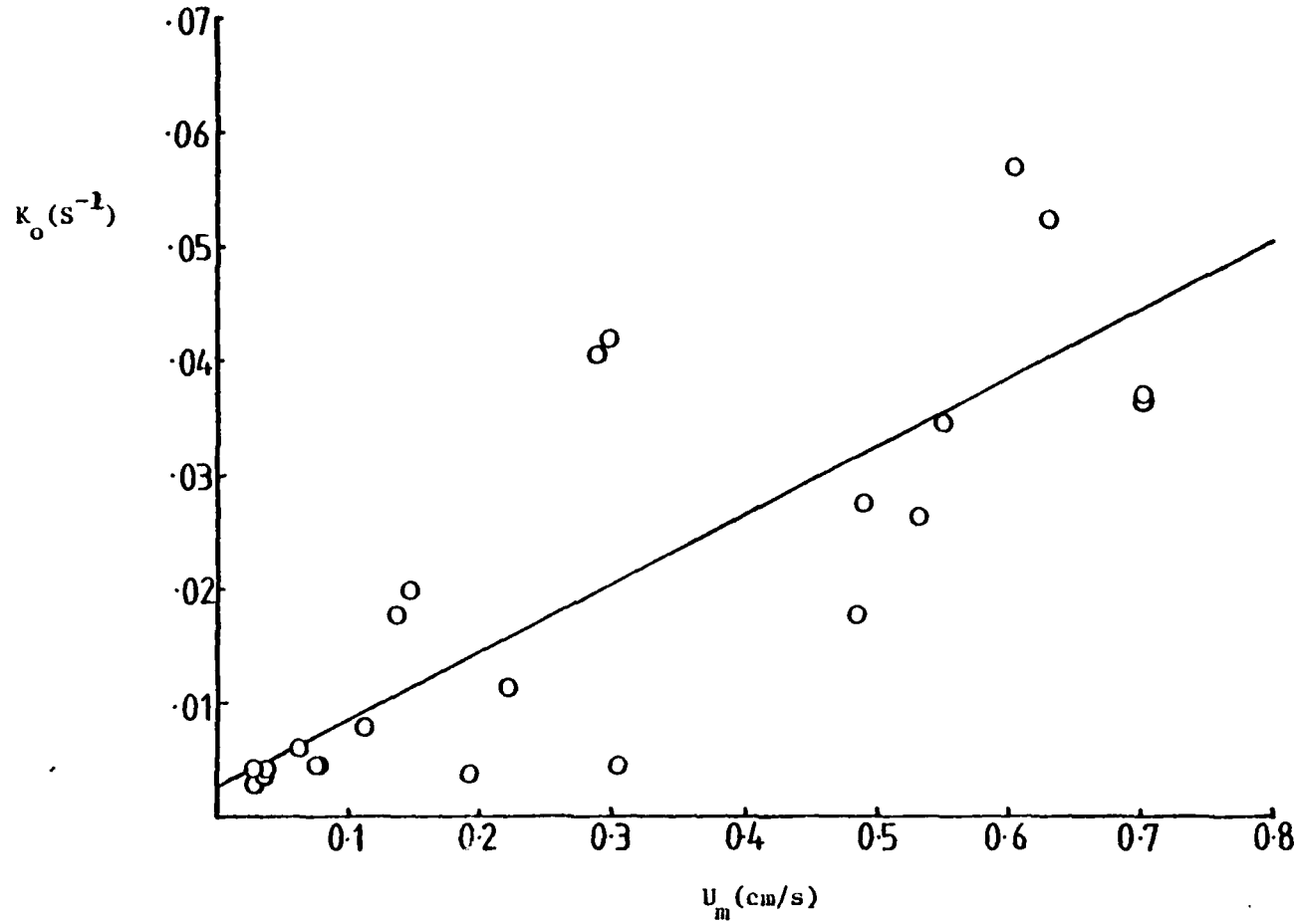

Figure 13. The variation in K_o with superficial melt velocity for a sandwich bed arrangement of 2" of 1/2" balls plus 10" of 1-3mm tabular alumina plus 2" of 1/2" balls.

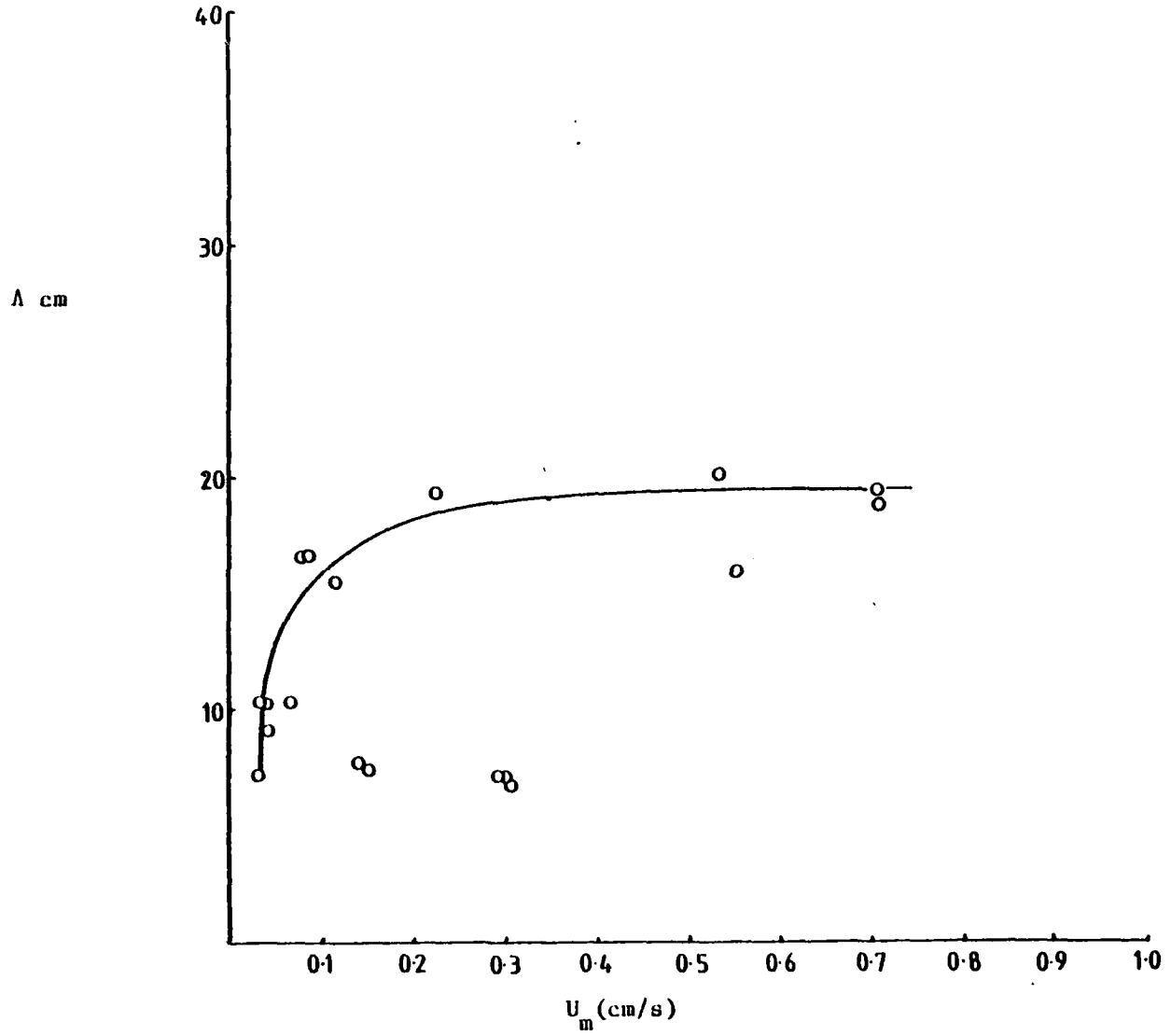

Figure 14. The variation in Λ with superficial melt velocity for a sandwich bed arrangement of 2" of 1/2" balls plus 10" of 1-3mm tabular alumina plus 2" of 1/2" balls.

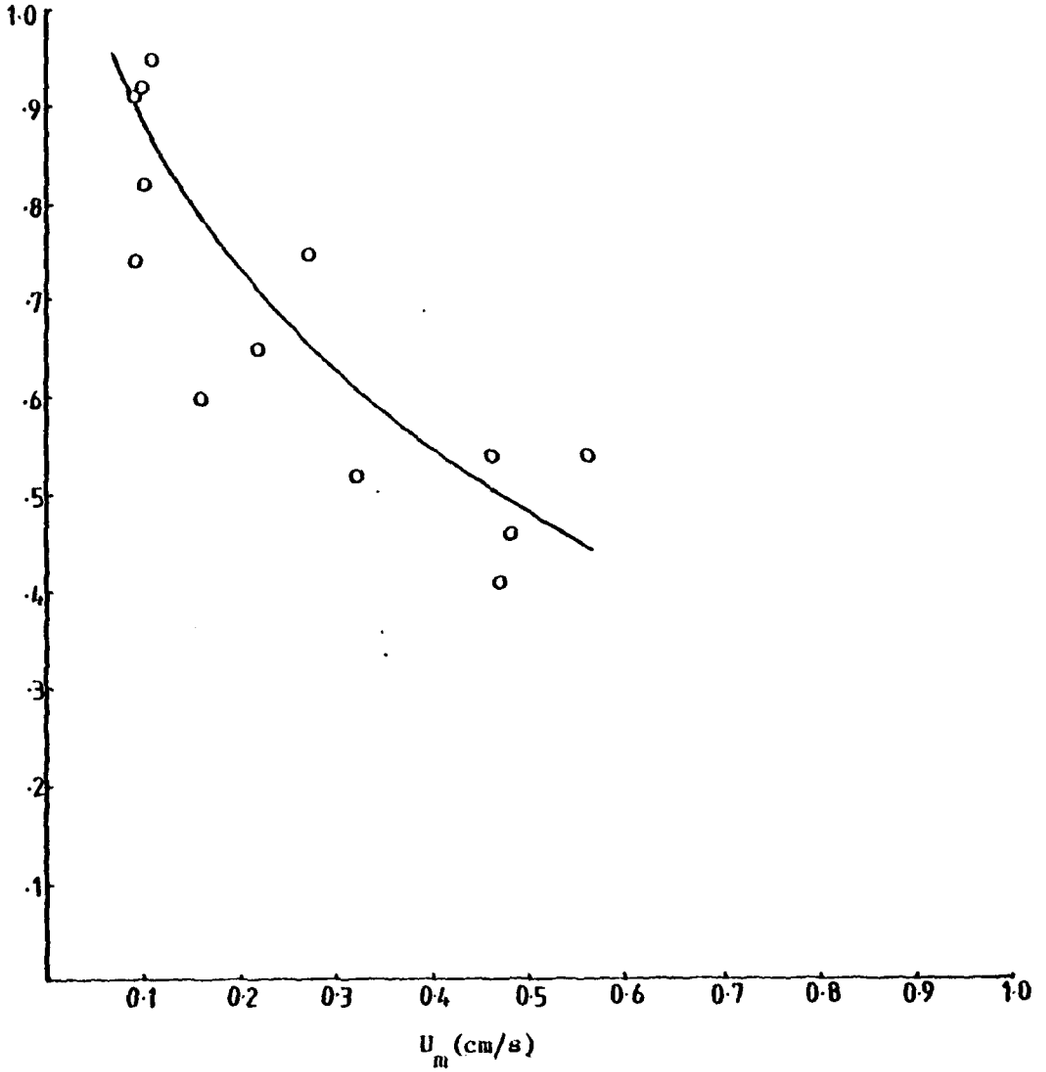

Figure 15. The variation in filtration efficiency with superficial melt velocity for a two inch bed of 1-3mm tabular alumina.

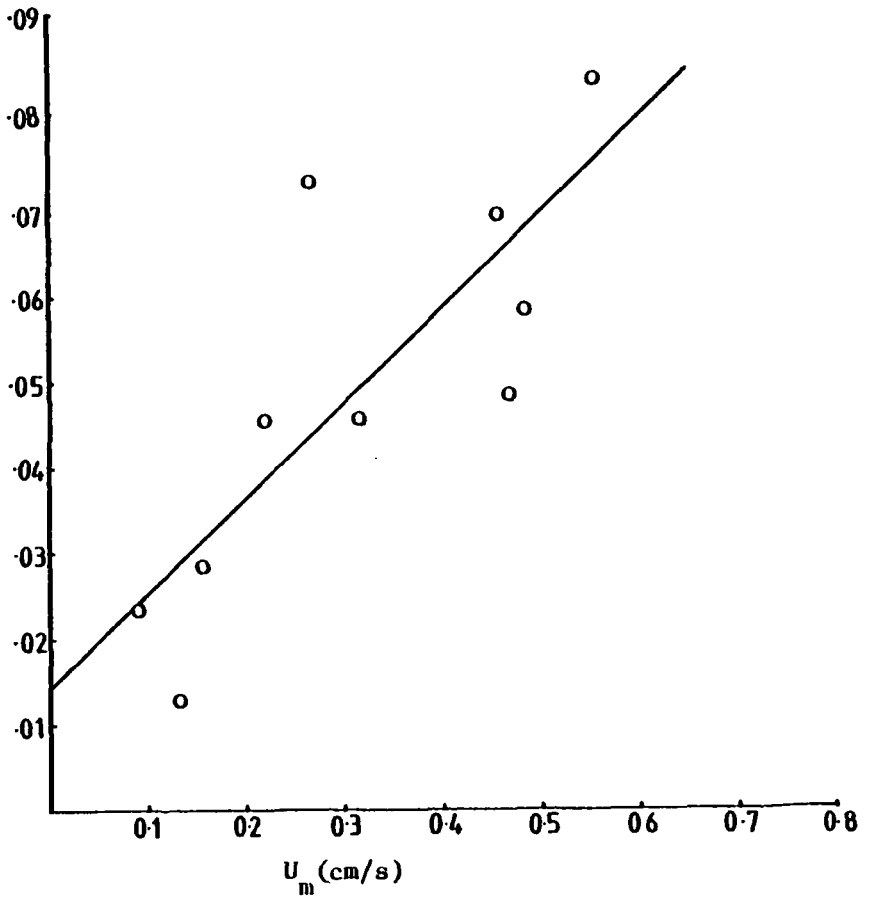

Figure 16. The variation in K_o with superficial melt velocity for a two inch bed of 1-3mm tabular alumina.

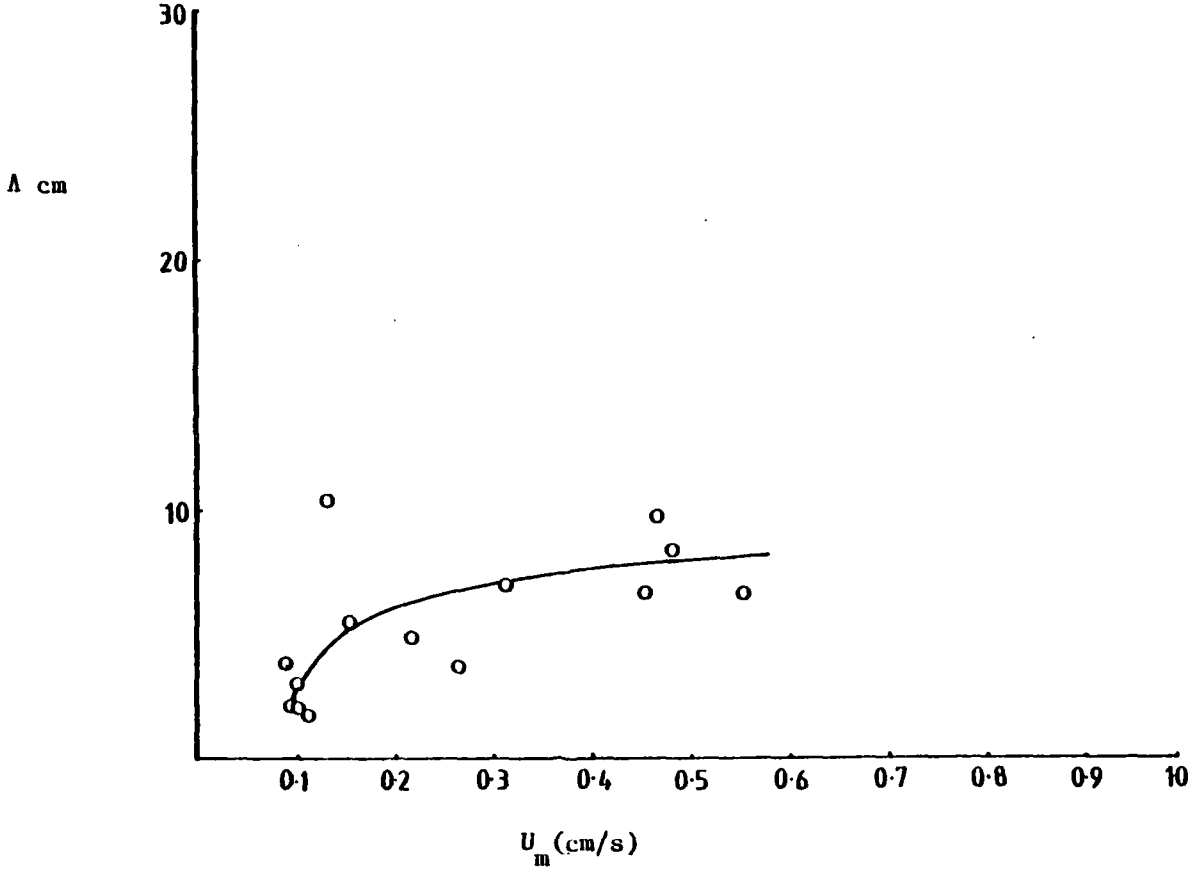

Figure 17. The variation of Λ with superficial melt velocity for a two inch bed of 1-3mm tabular alumina.

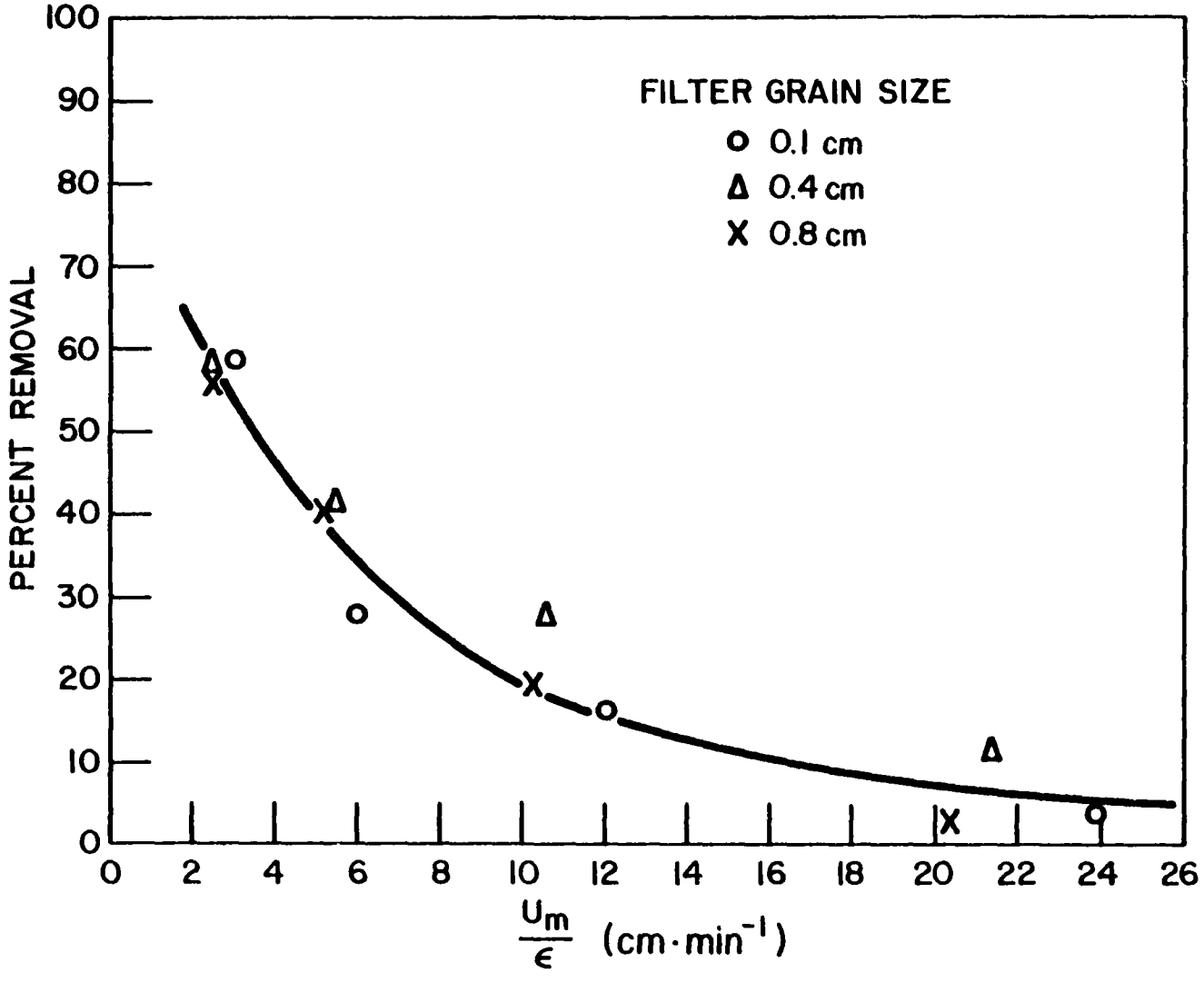

Figure 18. Filtration Efficiency as a function of suspension velocity for the diesel/hydrocarbon low temperature model.

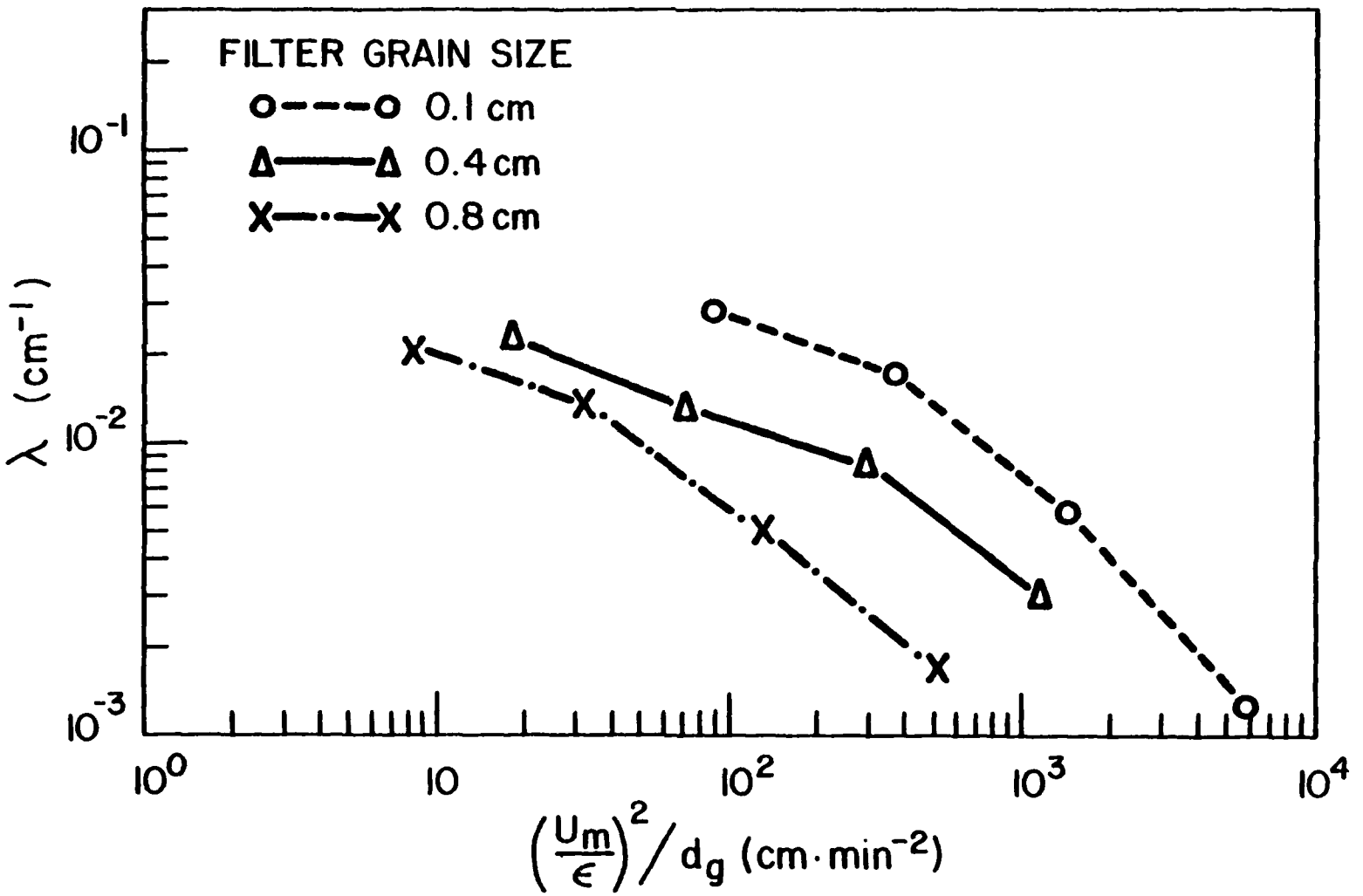

Figure 19. The parameter λ versus interstitial velocity for the low temperature model system.

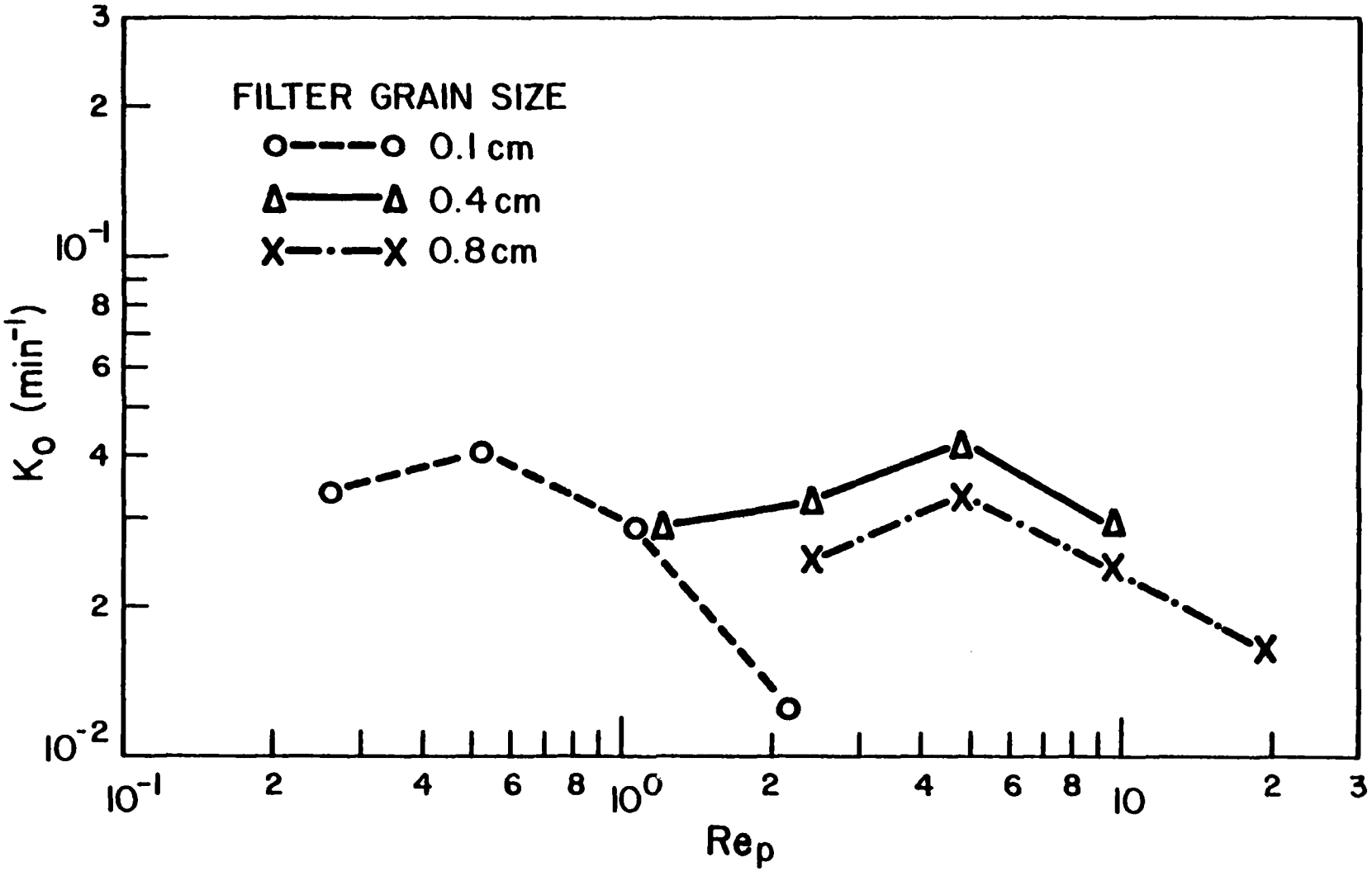

Figure 20. The parameter K_o versus interstitial velocity for tne low temperature model system (where the interstitial velocity = Um/ε. The bed porosity ε was measured as 42%).

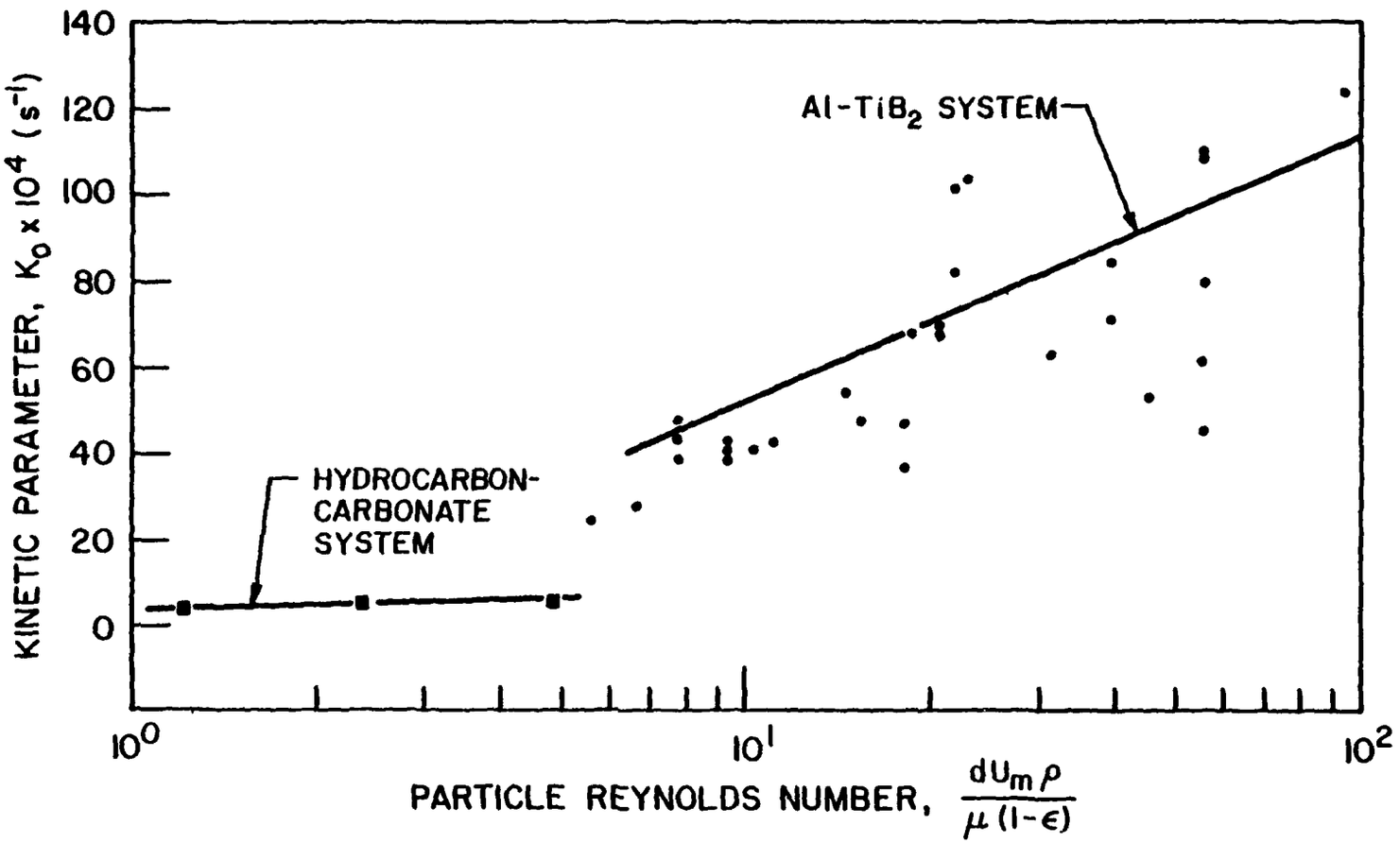

Figure 21. Effect of Particle Reynolds Number on the Kinetic Parameter

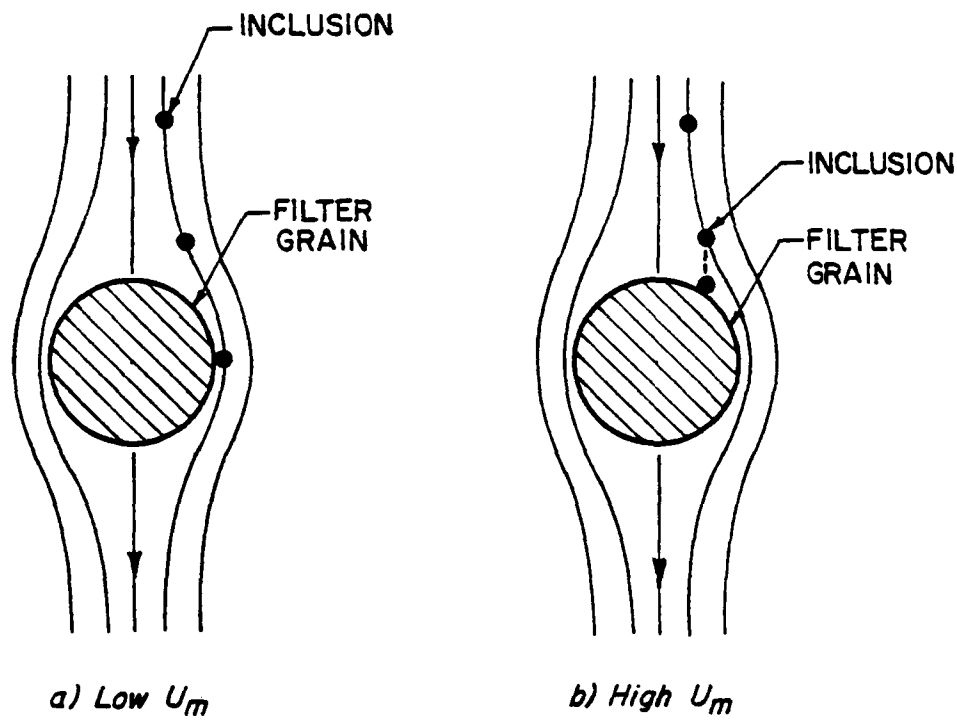

Figure 22. Effect of Velocity on Inclusion Trajectory near a Spherical Filter Grain.

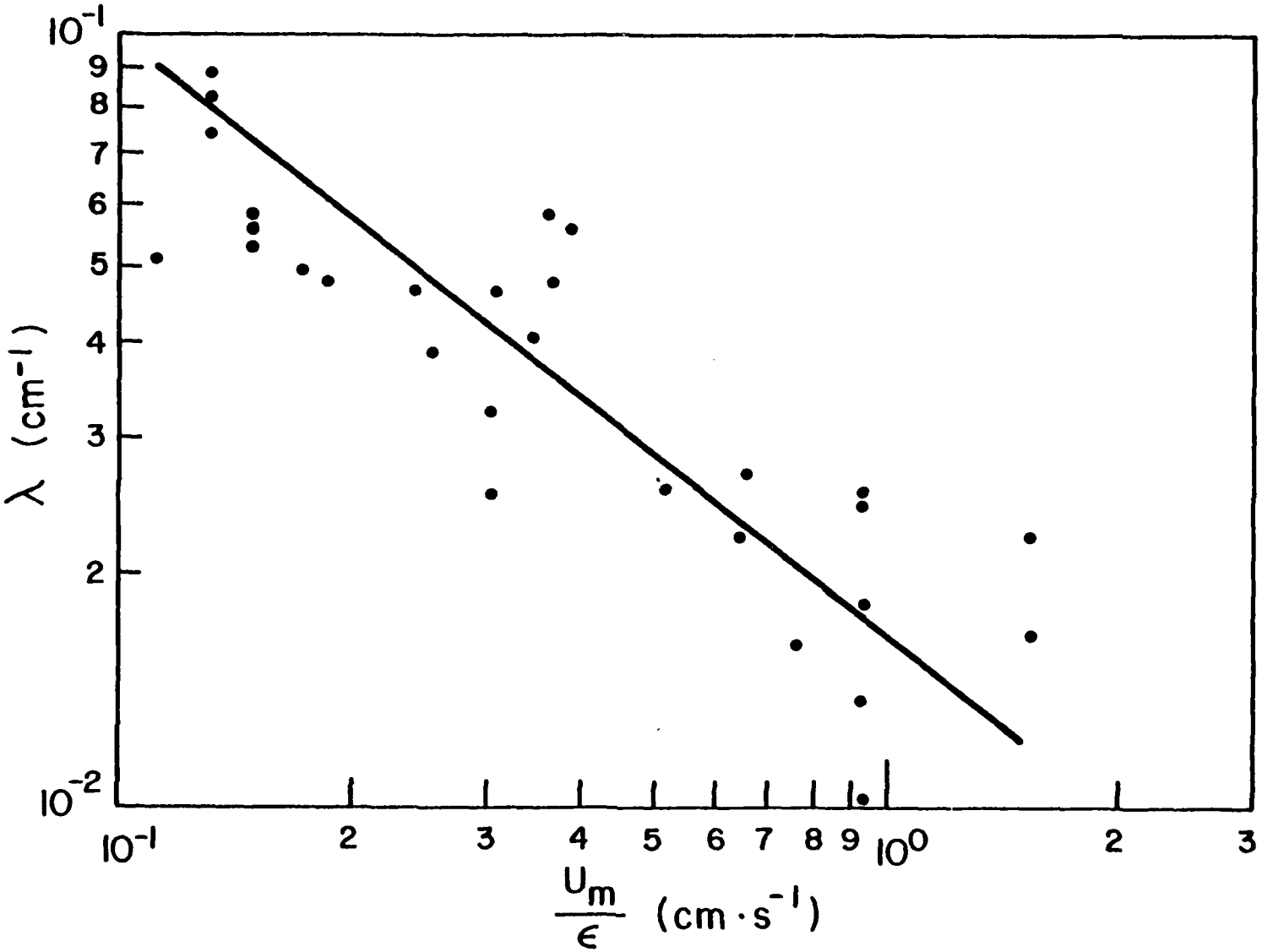

Figure 23. The filtration coefficient λ as a function of interstitial velocity where interstitial velocity = U_m/ϵ . For the initial 4mm work (see AMMRC TR-80-16).

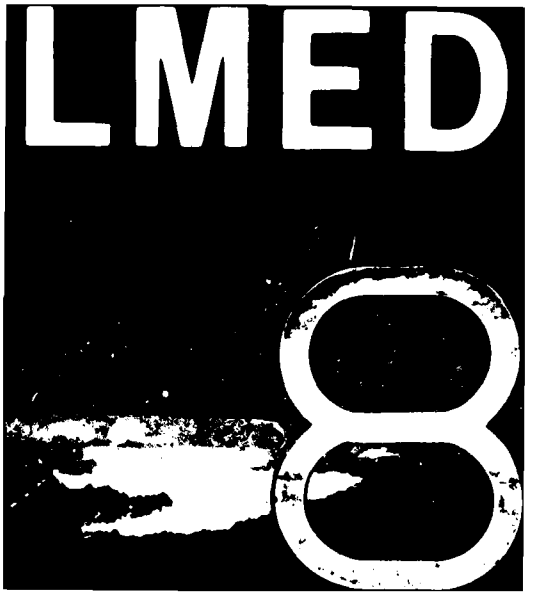
LMED
8